1 **Structural insights into SETD3-mediated histidine methylation on β-actin**

2

3 Qiong Guo[1,#], Shanhui Liao[1,#,*], Sebastian Kwiatkowski[2,#], Weronika Tomaka[2],

4 Huijuan Yu[1], Gao Wu[1], Xiaoming Tu[1], Jinrong Min[3,4], Jakub Drozak[2,*], Chao Xu[1,*]

5 1. Hefei National Laboratory for Physical Sciences at Microscale and School of Life

6 Sciences, University of Science and Technology of China, Hefei, Anhui, 230027,

7 People's Republic of China.

8 2. Department of Metabolic Regulation, Faculty of Biology, University of Warsaw,

9 Warsaw, Poland.

10 3. Structural Genomics Consortium, University of Toronto, 101 College St., Toronto,

11 Ontario, M5G 1L7, Canada.

12 4. Department of Physiology, University of Toronto, Toronto, Ontario, M5S 1A8,

13 Canada.

14 #: These authors contributed equally to this work.

15 Running title: Structure of SETD3 bound to a β-actin fragment

16 *: To whom correspondence should be addressed:

17 Chao Xu, xuchaor@ustc.edu.cn; Jakub Drozak, jdrozak@biol.uw.edu.pl;

18 Shanhui Liao, ajsod@mail.ustc.edu.cn.

19 **Keywords:** X-ray crystallography, post translational modifications, β-actin, SET

20 domain, N^3-methylhistidine

21

22

23

24

25

26

27

28

29

30

31 **ABSTRACT**

32 SETD3 is a member of SET (Su(var)3-9, Enhancer of zeste, and Trithorax) domain

33 protein superfamily and plays important roles in hypoxic pulmonary hypertension,

34 muscle differentiation, and carcinogenesis. In a previous paper (*Kwiatkowski et al.*

35 2018), we have identified SETD3 as the actin-specific methyltransferase that

36 methylates the N^3 of His73 on β-actin. Here we present two structures of

37 *S*-adenosyl-L-homocysteine-bound SETD3 in complex with either an unmodified

38 β-actin peptide or its His-methylated variant. Structural analyses supported by the

39 site-directed mutagenesis experiments and the enzyme activity assays indicated that

40 the recognition and methylation of β-actin by SETD3 is highly sequence specific, and

41 both SETD3 and β-actin adopt pronounce conformational changes upon binding to

42 each other. In conclusion, the structural research uncovers the molecular mechanism

43 of sequence-selective histidine methylation by SETD3, which not only throws light on

44 protein histidine methylation phenomenon, but also facilitates the design of small

45 molecule inhibitors of SETD3.

46

47 **INTRODUCTION**

48 Microfilaments are the building blocks of cytoskeleton and are made up of actin

49 proteins (dos Remedios et al., 2003; Theriot and Mitchison, 1991). There are six actin

50 isoforms in mammalian cells that are characterized based on different expression

51 profiles and cellular functions, including $\alpha_{skeletal}$-, $\alpha_{cardiac}$-, α_{smooth}-, β_{cyto}-, γ_{cyto}-, and

52 γ_{smooth}- actins (Gunning et al., 1983; Herman, 1993; Perrin and Ervasti, 2010). Among

53 them, β-actin is ubiquitously expressed and plays critical roles in a wide variety of

54 cellular functions, such as cytoskeleton formation, cell motility and maintenance of

55 cell stability (Leterrier et al., 2017; Nudel et al., 1983).

56

57 Many different types of post-translational modifications (PTMs) have been

58 found in actin protein, including acetylation, methylation, SUMOylation and

59 ubiquitination (Terman and Kashina, 2013). N^3-methylation of His73 in β-actin has

60 been of special interest since its identification in 1967 (Johnson et al., 1967), which

61   seems to be not only due to an extreme evolutionary conservation of this PTM–

62   methylated His is present in almost all eukaryotic actins, but mainly because the

63   methylation of H73 decreases the hydrolysis rate of the actin-bound ATP (Kabsch et

64   al., 1990), as evidenced by the higher ATP exchange rate in the actin-H73A mutant

65   (Nyman et al., 2002).

66

67   Although the presence of actin-specific methyltransferases was shown in rabbit

68   muscles decades ago (Raghavan et al., 1992; Vijayasarathy and Rao, 1987), the

69   molecular identity of this enzyme has long been unknown. Recently, we and others

70   identified SETD3 as the actin-specific histidine *N*-methyltransferase that specifically

71   catalyzes the methylation of actin at His73 (Kwiatkowski et al., 2018; Wilkinson et al.,

72   2019). SETD3 is a member of SET domain family, which is a ~130 aa motif initially

73   identified in Drosophila proteins, with its acronym derived from three histone lysine

74   methyltransferases, **S**u(var)3-9, **E**nhancer of zeste, and **T**rithorax (Dillon et al., 2005).

75   Thus far, most histone lysine methyltransferases contain a SET domain, however,

76   some exceptions include DOT1L (Min et al., 2003), METTL12 (Rhein et al., 2017),

77   and METTL21B (Malecki et al., 2017), among others. Before SETD3 was identified

78   as an actin-specific histidine methyltransferase, SET domain proteins had been known

79   to act as lysine methyltransferases, transferring a methyl moiety from the methyl

80   donor S-Adenosyl methionine (AdoMet) to the substrates to generate the methylated

81   form, with *S*-adenosyl-L-homocysteine (AdoHcy) as the co-product (Dillon et al.,

82   2005).

83

84   Since (i) SETD3 has been previously identified as a histone methyltransferase

85   that methylates histone H3 at Lys4 and Lys36 (Eom et al., 2011; Wagner and

86   Carpenter, 2012) and (ii) the results of our preliminary experiments with the use of

87   isothermal calorimetry titration (ITC) and mass spectrometry revealed that SETD3

88   binds to and methylates a β-actin peptide containing His73 (66-88), but not H3K4

89   (1-23) or H3K36 (25-47) peptides, we crystallized and solved two structures of

90   AdoHcy-bound SETD3 in complex with either His73 peptide or 3-methylhistidine

91 (His73me) one to understand the molecular mechanism of actin histidine methylation

92 by SETD3.

93

94   With the two solved β-actin peptide-SETD3 structures, we uncover that SETD3

95 recognizes a fragment of β-actin in a sequence-dependent manner and utilizes a

96 specific pocket to catalyze the N^3-methylation of His73. Moreover, a comprehensive

97 structural, biochemical and enzymatic profiling of SETD3 allows us to pinpoint its

98 key residues important for substrate recognition and subsequent methylation.

99 Therefore, the structural research, supplemented by biochemical and enzymatic

100 experiments, not only provides insights into the catalytic mechanism of SETD3, but

101 also will facilitate the design of specific inhibitors of SETD3 enzyme.

102

103 **RESULTS**

104 **SETD3 binds to and methylates β-actin**

105 Since SETD3 was identified as a histidine methyltransferase that methylates His73 of

106 β-actin (Kwiatkowski et al., 2018, Wilkinson et al., 2019), we purified the core region

107 of SETD3 (aa 2-502) and studied by ITC its binding to a His73-containing fragment

108 of β-actin (aa 66-88) (Figures 1A). The ITC binding experiment showed that SETD3

109 bound to the β-actin peptide with a Kd of 0.17 μM (Figure 1B and Table 1). Given

110 that SETD3 was also reported to be a putative lysine methyltransferase that

111 methylates Lys4 and Lys36 of histone H3 (Eom et al., 2011), we also verified the

112 binding of SETD3 to two different histone peptides, H3K4(1-23) and H3K36(25-47),

113 and found that neither of them binds to SETD3 (Table 1).

114

115   Furthermore, we tested the activity of SETD3 on β-actin(66-88), H3K4(1-23), and

116 H3K36(25-47) by mass spectrometry, and we found that SETD3 methylates β-actin

117 peptide (Figure 1–figure supplement 1A), but does not modify either H3K4 or H3K36

118 (Figure 1–figure supplement 1B-1C). No methylated product was detected for any of

119 above peptides in the presence of AdoMet without the addition of SETD3 (Figure

120 1–figure supplement 1A-1C). Moreover, SETD3 did not methylate β-actin(66-88)

121   H73A mutant, although the mutant peptide bound to SETD3 only ~2.5-fold weaker

122   than the wild type one (0.45 μM vs. 0.17 μM) (Figure 1B and Figure 1–figure

123   supplement 1D). Collectively, the peptide binding experiments and mass spectrometry

124   data indicate that SETD3 specifically binds to the β-actin peptide and methylates it at

125   His73.

126

127   **Overall structure of SETD3**

128   To uncover the mechanisms underlying recognition and methylation of β-actin by

129   SETD3, we attempted to crystalize AdoMet-bound SETD3 with full length β-actin,

130   but failed to obtain diffractable crystals. By using the core region of SETD3(2-502)

131   with the β-actin peptide (66-88), we succeeded in the crystallization of the complex

132   and obtained a 1.95 Å structure of AdoHcy-bound SETD3 (2-502) with β-actin (66-88)

133   (Table 2, Figure 1–figure supplement 2A, Figure 1–figure supplement 3). There are

134   four molecules in a crystallographic asymmetric unit and residues 22-501 of SETD3

135   and 66-84 of β-actin are visible in the complex structures (Figure 1–figure supplement

136   4A). Based on the density map, we found that His73 of β-actin had been methylated

137   in the structure (Figure 1–figure supplement 5A), although we used an unmethylated

138   peptide. The reason could be that SETD3 bound to the methyl donor AdoMet from *E.*

139   *coli*, which we used to express our protein, and that the AdoMet-bound SETD3

140   methylated the peptide at His73 during crystallization. Therefore, this complex

141   represents a snapshot of the post-methyl transfer state, which prompted us to

142   crystallize the substrate-bound enzyme.

143

144   To avoid the methylation reaction, SETD3 was purified by adding 5-fold excess

145   of AdoHcy in the buffer to compete off AdoMet. Then the non-methylated peptide

146   was mixed with the purified SETD3 to form the complex. The complex was

147   crystallized and solved at a resolution of 2.15 Å (Table 2). There are two molecules in

148   a crystallographic asymmetric unit (Figure 1–figure supplement 4B). In this structure,

149   the density map of the peptide indicates that it was unmodified, suggesting that

150   methylation did not occur (Figure 1–figure supplement 5B). The complex structure

151   hereby reflects the image of the pre-methyl transfer state.

152

153   In both structures, the SETD3 core region adopts a V-shape architecture and is

154   composed of N-SET (N-terminal to the SET domain), SET, iSET (an insertion in the

155   SET domain), and C-SET (C-terminal to the SET domain) domains (Figure 1C). The

156   N-terminal lobe consists of the N-SET (α1-α3), SET (β1-β12), and iSET (α4-α11)

157   domains (Figure 1–figure supplement 2A, Figure 1–figure supplement 3). The N-SET

158   domain consists of three α helices (α1-α3), and encompasses the SET and iSET

159   domains (Figure 1–figure supplement 2A, Figure 1–figure supplement 3). While α1

160   and α2 of N-SET form a 4-helix bundle with α10-α11 of iSET, α3 of N-SET is

161   localized at the SET-iSET interface and comes into contact with the anti-parallel β

162   strands (β1-β2) of SET and α8 of iSET (Figure 1C, Figure 1–figure supplement 3).

163   The SET domain adopts a canonical SET domain fold similar to that of LSMT

164   (Trievel et al., 2002), with twelve β strands arranged into four anti-parallel β sheets

165   (β1-β2, β3-β11, β4-β10-β9, β5-β7-β6) and one parallel β sheet (β8-β12) (Figure

166   1–figure supplement 2A, Figure 1–figure supplement 3). The iSET domain is a helical

167   region (α4-α11) inserted between β5 and β6 of the SET domain (Figure 1–figure

168   supplement 2A, Figure 1–figure supplement 3). The C-terminal lobe, only consisting

169   of the C-SET domain, is almost entirely helical (α12-α19) except two anti-parallel

170   strands (β13-β14), with α12 and the N-terminal end of α19 packed against α10 and α9

171   of iSET, respectively (Figure 1–figure supplement 2A, Figure 1–figure supplement 3).

172   Consistently, a database search using the DALI server (Holm and Rosenstrom, 2010)

173   revealed that the overall fold of SETD3 is highly similar to those of LSMT (Z-core:

174   31.4, RMSD: 3.8 Å for 425 Cα atoms) and SETD6 (Z-core: 28.7, RMSD: 2.8 Å for

175   421 Cα atoms) despite the low sequence identities (24%-25%).

176

177   **AdoHcy binding pocket within SETD3**

178   In both complex structures, SETD3 binds AdoHcy in a cleft formed between SET and

179   C-SET and buttressed by iSET at the bottom (Figure 1C). Specifically, the adenine

180   ring of AdoHcy is sandwiched between the side chain of Glu104 and the aromatic ring

181 of Phe327, forming stacking and π-π interactions, respectively (Figure 1–figure

182 supplement 6A). The AdoHcy N^6 and N^7 atoms are hydrogen bonded to the main

183 chain carbonyl and amide groups of His279, respectively, while the AdoHcy C^8 atom

184 forms one C-H...O hydrogen bond with the hydroxyl group of Tyr313 (Figure

185 1–figure supplement 6A).

186

187   In addition to the adenine specific interactions, the ribose O3' and O4' atoms of

188 AdoHcy form hydrogen bonds with the main chain carbonyl of Ser325 and the side

189 chain carboxyl of Asn278, respectively (Figure 1–figure supplement 6A). The side

190 chain carboxyl of Asn278 makes another hydrogen bond with the AdoHcy amide,

191 while the latter is also H-bonded to the main chain carbonyl of Phe106 (Figure

192 1–figure supplement 6A). The AdoHcy carboxylate forms four hydrogen bonds with

193 SETD3 residues, one with the main chain amide of Phe106, one with the guanidino

194 group of Arg254, and the other two with the guanidino group of Arg75 (Figure

195 1–figure supplement 6A). All AdoHcy binding residues are conserved in other SETD3

196 orthologs, suggesting a conserved function of SETD3 (Figure 1–figure supplement

197 2A).

198

199   The AdoHcy binding mode of SETD3 is similar to those observed in some other

200 SET domain structures, such as those of LSMT (Trievel et al., 2002) and SETD6

201 (Chang et al., 2011) (Figure 1–figure supplement 6B-6C). Among these AdoHcy

202 binding residues, Asn278, His279 and Phe327 are conserved in LSMT and SETD6,

203 while Glu104 and Arg254 are conserved only in LSMT, but not in SETD6 (Figure

204 1–figure supplement 2B, Figure 1–figure supplement 6B-6C). Arg75 is an AdoHcy

205 binding residue only found in SETD3 (Figure 1–figure supplement 2B).

206

207 **β-actin binding mode of SETD3**

208 In both complexes, the β-actin peptide lies in a narrow groove formed by SET, iSET

209 and C-SET, with the unmodified or methylated His73 residue accommodated in a

210 pocket composed of α11 of iSET, β6 and β12 of SET, and α12 of C-SET, and further

211   buttressed by η5 of SET (Figure 1C, Figure 2A). When superimposing our

212   substrate-bound complex structure with the previously determined AdoMet-SETD3

213   binary structure (PDB id: 3SMT) on SETD3, we found that, despite the overall

214   structural similarity between two SETD3 structures (with a RMSD of 0.66 Å in Cα

215   positions), the region containing two β-sheets of the SET domain (β4-β10-β9 and

216   β3-β11) takes a conformational change upon peptide binding, due to its direct

217   interactions with the N-terminal end of the peptide, with the three loops preceding β4,

218   β9 and β11 shift 4.2 Å, 4.4 Å and 6.8 Å towards the peptide, respectively (Figure

219   1–figure supplement 7). The detailed interactions between SETD3 and the N-terminal

220   end of the peptide will be described in the following section.

221

222   **A unique histidine recognition pocket in SETD3 confers to its histidine**

223   **methyltransferase activity**

224   In the substrate complex, residues Leu67-Glu83 of the peptide are visible, with His73

225   occupying a hydrophobic pocket (Figure 2A). The main chain of His73 forms several

226   hydrogen bonds with SETD3, with its main chain amide, Cα and main chain carbonyl

227   H-bonded to the main chain carbonyl of Tyr313, the side chain carboxyl of Asn256,

228   and the guanidino of Arg316, respectively (Figure 2A). The imidazole ring of His73 is

229   parallel to the aromatic ring of Tyr313, with its orientation determined by two

230   hydrogen bonds, one between the N^1 atom of the ring and the guanidino of Arg316

231   mediated by a water molecule, and the other between the N^3 atom of the ring and the

232   main chain carbonyl of Asp275 (Figure 2A). In addition to the stacking interactions

233   with Tyr313, His73 also makes hydrophobic contacts with Trp274 and Ile311. The

234   distance between the N^3 atom of His73 and the sulfur atom of the AdoHcy is 3.7 Å,

235   suggesting that it represents well the pre-methyl transfer state (Figure 2A).

236

237   In the product complex, the residues Leu67-Lys84 and the main chain of Ile85 of

238   the peptide are visible, with His73 methylated to His73me (Figure 1–figure

239   supplement 8). Despite the fact that the methylated peptide adopts a 3^{10} helix at its

240   C-terminal end, the two complexes are highly similar, with a RMSD of 0.19 Å over

241 protein Cα atoms and a RMSD of 0.32 Å over peptide Cα atoms. In the product

242 complex, His73me is inserted into the same pocket of SETD3 as shown in the

243 substrate complex and the distance between the installed methyl group of His73 and

244 the sulfur atom of the AdoHcy is 3.2 Å, with its density map distinguishable from that

245 of unmodified histidine (Figure 2B).

246

247   The superposition of the two complexes clearly indicates that the hydrogen bonds

248 between the main chain of His73me and the main chain carbonyl of Tyr313 and the

249 guanidino of Arg316 are intact after methylation (Figure 2B). However, the imidazole

250 ring of His73me is rotated by ~90° compared to that of the unmodified His73, with its

251 C^4H pointing toward the ring of Tyr313 (Figures 2B-2C) and its N^1 atom hydrogen

252 bonded to the side chain carboxyl group of Asn256 (Figure 2B).

253

254   When comparing SETD3 with the other SET domain containing lysine

255 methyltransferases, we found that there are two main reasons that SETD3 is not likely

256 to be a lysine methyltransferase. Firstly, the histidine binding pocket of SETD3 is too

257 shallow to accommodate the aliphatic side chain of a lysine. Replacement of His73

258 with a lysine, would not only disrupt the water mediated hydrogen bond between N^1

259 of His73 and Arg316, but could also lead to the steric clash between the aliphatic side

260 chain of lysine and the main chain of the bottom carbonyl cage residue, Asp275.

261 Secondly, the phenylalanine of LSMT and SETD6 that makes cation-π interaction

262 with the lysine, is replaced by an asparagine (Asn256) in SETD3, and Asn256 is

263 critical for substrate binding and histidine methylation (Figures 2A-2B and Figure

264 1–figure supplement 2A). Therefore, this substitution establishes the imidazole

265 ring-specific interaction with histidine by impairing the lysine specific interaction.

266

267 **SETD3 exhibits extensive interactions with β-actin**

268 In both complexes, peptide residues flanking His73 or His73me also interact

269 extensively with the N-terminal lobe of SETD3, with Leu67-Glu72 and Gly74-Glu83

270 mainly contacting the SET and iSET motifs, respectively (Figure 2–figure supplement

271   1, Figure 2–figure supplement 2). Leu67 and Pro70 of β-actin make hydrophobic

272   contacts with Ile284 of SETD3 and there are additional hydrophobic interactions

273   between Tyr69 of β-actin and Pro259, Tyr288 and Leu290 of SETD3 (Figure 2–figure

274   supplement 1, Figure 2–figure supplement 2). Two main chain hydrogen bonds are

275   formed between Tyr69 of β-actin and Tyr288 of SETD3, and between Ile71 of β-actin

276   and Thr286 of SETD3, which induces the shift of the two sheets (β4-β10-β9 and

277   β3-β11) in SETD3 as mentioned above (Figure 1–figure supplement 7). Ile71 of actin

278   also makes hydrophobic interactions with Ile258, Ile271, Trp274, Thr286, Tyr288 and

279   Cys295 of SETD3 (Figure 2–figure supplement 1, Figure 2–figure supplement 2). Of

280   note, Leu283-Thr285 of SETD3 adopts a β strand in the structure of AdoMet bound

281   SETD3 without peptide (PDB: 3SMT), but decomposes upon binding to the

282   N-terminal side of β-actin, which shortens the β9 strand of SETD3 in the

283   peptide-bound structure (Figure 1–figure supplement 7). The side chain carboxylate

284   group of Glu72 forms one hydrogen bond with the guanidino group of Arg316, which

285   is the only C-SET domain residue that contacts the N-terminal side of the β-actin

286   peptide (Figure 2–figure supplement 1, Figure 2–figure supplement 2).

287

288   Regarding the residues C-terminal to His73 of β-actin, the main chain amide

289   group of Gly74 is hydrogen bonded to the main chain carbonyl group of Gln255,

290   while the side chain of Val76 stacks with the imidazole ring of His324 (Figure

291   2–figure supplement 1, Figure 2–figure supplement 2). In contrast to Gly74 and Val76,

292   the Ile75 side chain is solvent-exposed and is thereby not involved in the interactions

293   with SETD3 (Figure 2–figure supplement 1). Thr77 not only makes hydrophobic

294   contact with Leu268, but also forms two hydrogen bonds through its hydroxyl group

295   with the side chain amide groups of Asn154 and Gln255, respectively (Figure

296   2–figure supplement 1, Figure 2–figure supplement 2). The side chain amide group of

297   Asn154 makes another hydrogen bond with the main chain carbonyl of Asn78. The

298   indole ring of Trp79 is inserted into an open hydrophobic pocket composed of Ile155,

299   Val248, Val251 and Met252, with its main chain carbonyl H-bonded to the side chain

300   amide of Gln216, while the carboxyl group of Asp80 is hydrogen bonded to the side

301   chain amide of Arg215 (Figure 2–figure supplement 1, Figure 2–figure supplement 2).

302   Asp81 of β-actin forms three hydrogen bonds with SETD3, one with the side chain

303   amide of Gln216 and two with the guanidino group of Arg215 (Figure 2–figure

304   supplement 1, Figure 2–figure supplement 2). Of note, the peptide sequence is also

305   conserved in α- and γ-actin proteins, suggesting that SETD3 might also recognize and

306   methylate other actin isotypes.

307

Key residues of SETD3 involved in β-actin binding and methylation

309   To evaluate the roles of the SETD3 residues around the active site in β-actin

310   methylation, we made several single mutants and compared quantitatively their

311   binding affinities to the β-actin peptide by ITC. While all SETD3 mutants displayed

312   weaker binding affinities towards the peptide, R215A and R316A exhibited the most

313   significantly reduced binding affinities by 21- and 42- fold, respectively (Table 1).

314   Our complex structures showed that both Arg215 and Arg316 make several hydrogen

315   bonds with β-actin (Figure 2B, Figure 2–figure supplement 1), implicating that they

316   play a critical role in substrate recognition (Table 1). N256A also reduces the β-actin

317   binding affinity by 12-fold (Kd = 2.1 μM) (Table 1), which disrupts not only the

318   hydrogen bond to the main chain of the His73 Cα atom (Figure 2A), but also the one

319   to the N^1 atom of His73me (Figure 2B). In the substrate complex, the imidazole ring

320   of His73 stacks with the aromatic ring of Tyr313, with the N^3 atom of His73 in

321   proximity to the hydroxyl group of Tyr313 (Figure 2A). The hydroxyl group of

322   Tyr313 partially neutralizes the charge of N^3, as verified by the fact that mutating

323   Tyr313 to phenylalanine diminishes binding affinity by 17-fold (Kd = 3.0 μM) (Table

324   1). A similar favorable charge-charge interaction was also observed in the structure of

325   Gemin5 bound to m^7G base (Xu et al., 2016),

326

327   Given that the β-actin peptide interact with SETD3 via flanking sequences of

328   His73, we performed mutagenesis and ITC studies to corroborate the roles of Tyr69,

329   Ile71, Asp80, Asp81, and Met82. Tyr69, Ile71 and Met82 of β-actin contact SETD3

330   via hydrophobic interactions, and replacing either of them by alanine dramatically

331   reduces the SETD3 binding affinity by 5-90 fold (Table 1). Consistent with the fact

332   that both Asp80 and Asp81 of β-actin form hydrogen bonds with SETD3, D80A and

333   D81A impair the binding to SETD3 by 20- and 11-fold, respectively (Table 1). The

334   interactions of Asp81 and Met82 of β-actin with SETD3 also explains why truncation

335   of Asp81-His88 of the peptide reduces the binding to SETD3 by ~17-fold (Figure

336   2–figure supplement 1, Table 1). Taken together, the flanking sequences of His73,

337   rather than His73 itself on the β-actin peptide, are critical for binding to SETD3,

338   suggesting that the substrate recognition by SETD3 is highly sequence-selective.

339

340   To gain further insights into how substrate recognition by SETD3 affects

341   subsequent histidine methylation, we used the mass spectrometry to compare the

342   activity of the above mentioned SETD3 mutants with that of the wild type protein in

343   the presence of AdoMet. The mass spectrometry data indicate that the peaks of

344   products generated by the four SETD3 mutants (R215A, N256A, Y313F, and R316A)

345   were much lower than that observed for wild type SETD3 (Figure 1–figure

346   supplement 1E), suggesting that these mutants displayed weaker histidine methylation

347   activity.

348

349   **Activity of SETD3 enzyme and its mutant variants towards β-actin protein**

350   To verify the identification of key catalytic residues of SETD3, and to analyze the

351   roles of substrate recognition residues in catalysis, we determined the kinetic

352   properties of the wild-type and mutant variants of purified recombinant SETD3 in the

353   presence of homogenous full length recombinant human β-actin**.** All enzyme assays

354   were performed in the presence of *E. coli* AdoHcy nucleosidase and *B. subtilis*

355   adenine deaminase to prevent the accumulation of AdoHcy in the reaction mixture

356   (Dorgan et al., 2006). As shown in Table 3, the wild-type SETD3 has a very high

357   affinity towards both AdoMet ($K_M \approx 0.1$ μM) and β-actin ($K_M \approx 0.5$ μM), though it

358   appeared as a sluggish catalyst, with k_{cat} equal to about 0.7-0.8 min^{-1}. All mutant

359   enzymes exhibited a reduced catalytic efficiency as indicated by k_{cat}/K_M, 2-400 fold

360   and 1.6-2000 fold for β-acint and AdoMet, respectively (Table 1), confirming the

361   importance of examined amino acid residues for the efficient catalysis.

362

363   Arg75 and Asn278 are both AdoMet binding residues and mutating either of them

364   to alanine severely impaired k_{cat} of the enzyme towards β-actin and AdoMet (c.f.

365   Table 3). Interestingly, although N256A and Y313F weakened the binding to β-actin

366   peptide by ~12- and ~17- fold, respectively (Table 1), both mutants displayed K_M

367   values (0.449 μM and 0.581 μM, respectively) comparable to that of wild type SETD3

368   (0.502 μM), probably owning to their much lower k_{cat} values (~26- and ~36-fold,

369   respectively) than wild type SETD3 (c.f. Table 3). For AdoMet, N256A and Y313F

370   both have a higher K_M (~6- and ~58-fold, respectively) and lower k_{cat} (~9- and

371   ~6-fold, respectively) than wild type enzyme. We also examined the kinetic properties

372   of N256D and N256Q, and found that for both β-actin and AdoMet, kinetic

373   parameters of N256Q are comparable to those of the wild type SETD3, while N256D

374   behaves similarly to N256A (Table 3). Taking into account that Asn256 and Tyr313 of

375   SETD3 interact mainly with His73 of β-actin, and not with AdoMet (Figures 2A-2B),

376   these results may imply that Asn256 and Tyr313 of SETD3 plausibly bind to His73 of

377   β-actin by favorably orienting its imidazole ring to facilitate the efficient transfer of

378   the methyl group from AdoMet to His73. The consequence of the N256A and Y313F

379   mutations is thus a decrease in the rate of "successful" methylation events that could

380   be partially overcome by an increase in AdoMet concentration.

381

382   In contrast to Asn256 and Tyr313, Arg215 and Arg316 of SETD3 contact flanking

383   sequences of His73. R215A and R316A, which impaired the binding of SETD3 to

384   β-actin peptide, also displayed higher K_M values (~2 fold for both) and lower k_{cat}

385   values (~3.5- and ~4.5-fold, respectively) for β-actin protein (Table 3), confirming

386   that those SETD3 residues involved in β-actin peptide recognition are also important

387   for efficient His73 methylation in the context of the full length β-actin.

388

389   We further investigated the pH-dependent activity of SETD3 towards full length

390   β-actin and found that SETD3 catalyzes the methylation of β-actin in a wide range of

391   pH (6.0-9.0), with its activity increasing with pH and reaching maximum at pH 9.0

392   (Figure 3). The detectable activity of SETD3 at neutral pH is consistent with the fact

393   that histidine deprotonation occurs at neutral pH, which facilitates the transfer of

394   methyl group from AdoMet to histidine. Like lysine, histidine deprotonation also

395   increases with pH, well explaining the higher activity of SETD3 in alkaline

396   conditions.

397

398   **DISCUSSION**

399   **Catalytic mechanism of SETD3**

400   As the major component of microfilament, actin participates in diverse cellular

401   processes. Different types of PTMs have been identified in actin, which play

402   important roles in mediating actin functions *in vivo*. (Terman and Kashina, 2013).

403   N^3-methylhistidine was identified in β-actin decades ago (Johnson et al., 1967) and

404   was postulated to mediate the polymerization and hydrolysis of actin filaments

405   (Kabsch et al., 1990). However, how the mark is incorporated, remains enigmatic.

406   Our identification of SETD3 as a histidine methyltransferase catalyzing the His73

407   methylation of β-actin, answers this unsolved question.

408

409   Although SETD3 contains a canonical SET domain and its AdoHcy binding

410   mode is similar to those observed in other SET domain lysine methyltransferases, the

411   predicted SET domain fold of SETD3 does not help to disclose the molecular

412   mechanisms of the substrate recognition and histidine methylation, since the SET

413   domain itself, as a short motif of ~110 aa, always requires iSET and C-SET domains

414   to complete its function (Chang et al., 2011; Trievel et al., 2002). Our solved

415   substrate- and product-bound structures of SETD3, provides an insight into the pre-

416   and post-methyl transfer states of the histidine methylation by the same enzyme. The

417   SETD3 structures, for the first time, uncover the molecular mechanism by which a

418   SET domain protein acts as the actin His73-specific methyltransferase.

419

420   Our structural analyses, assisted by mutagenesis and biochemical experiments,

421   suggest that the recognition of β-actin and subsequent catalysis by SETD3 is different

422   from those observed for other SET domain-containing lysine methyltransferases in

423   following aspects: i) the histidine recognition pocket of SETD3 is shallower and key

424   residues of SET3, which form hydrogen bonds with the His73 imidazole ring, are not

425   conserved in other SET proteins. (Figures 2A-2B, Figure 1–figure supplement 2B); ii)

426   In two solved SETD3 complex structures, the methylated histidine rotates its side

427   chain by 90° (Figure 2C); (iii) The recognition of β-actin by SETD3 is highly

428   dependent on the flanking sequences of His73 (Figure 2–figure supplement 1), which

429   is consistent with the high binding affinity between SETD3 and β-actin H73A peptide

430   (66-88) (Figure 1B). Although N^3-methylhistidine is also found in other proteins, such

431   as mammalian myosin (Johnson et al., 1967) and *Saccharomyces cerevisiae* Rpl3

432   (Webb et al., 2010), the sequence preference suggests that SETD3 probably works

433   only on His73 of β-actin, as well as on corresponding histidines in α- and γ-actins.

434   One implication is that no SETD3 ortholog is found in baker's yeast.

435

436   Previously, we identified *Carnosine N-methyltransferase 1* (*CARNMT1*) as the

437   gene coding for carnosine *N*-methyltransferase in mammals (Drozak et al., 2015),

438   which catalyzes N^1-methylation of the histidine imidazole ring of carnosine

439   (β-alanyl-L-histidine), an abundant dipeptide in skeletal muscle of vertebrates.

440   Recently, the structures of CARNMT1 bound to analogs of N^1-methylhistidine were

441   also reported (Cao et al., 2018), allowing us to compare the N^3-histidine methylation

442   by SETD3 with the N^1-histidine methylation by CARNMT1 through comparing two

443   complexes (Figures 2A and 2E). We found that SETD3 and CARNMT1 not only

444   adopt different folds and AdoHcy binding modes, but also display distinct histidine

445   recognition and catalysis mechanisms. Asp316 of CARNMT1 forms two hydrogen

446   bonds with the imidazole ring of the histidine to facilitate its deprotonation (Figure 2E)

447   (Cao et al., 2018). In the SETD3-substrate complex, His73 stacks with Tyr313 and is

448   hydrogen bonded to the main chain carbonyl group of Asp275 (Figure 2A), which

449   orients the His73 imidazole ring for efficient catalysis. Tyr313 of SETD3 plays

450   important roles in substrate recognition and subsequent histidine methylation,

451 supplemented by the mutagenesis, ITC binding experiments and enzymatic assays

452 (Table 1, Table 3). Finally, the 90-degree rotation of the His73me imidazole ring was

453 not found in CARNMT1-mediated histidine methylation.

454

455 **Implications of conformational changes of actin upon binding to SETD3**

456 In natively purified rabbit β-actin, His73 exists as the methylated form and it is

457 localized close to the phosphate groups of ATP binding to actin (Kabsch et al., 1990).

458 Although our complexes only contain a fragment of β-actin, they could still provide

459 clues to the role of SETD3 in mediating actin functions. The residues 66-84 of β-actin

460 consist of three β strands followed by an α-helix, however, the β-actin peptide adopts

461 an extended conformation upon binding to SETD3 (Figure 2–figure supplement 3),

462 suggesting that β-actin probably endures local structural remodeling during

463 methylation. Given that SETD3 is found to be co-purified with other factors, such as

464 the peptide release factor ERF3A (Kwiatkowski et al., 2018), SETD3 might require

465 the assistance of other protein(s) to acquire the methylation of actin His73.

466

467 **Conclusions**

468 In the current investigation, we have identified molecular mechanism of β-actin

469 methylation by SETD3 and indicated that the enzyme displays a very high substrate

470 specificity towards β-actin His73. Since the overexpression of SETD3 was recently

471 reported to be associated with cancer malignancy (Cheng et al., 2017), the high-

472 resolution complex structures of SETD3 might be helpful for a better understanding

473 of the role of actin histidine methylation in human cancer, as well as they could

474 provide a structural basis for designing specific SETD3 inhibitors in the near future.

475

476   During the peer review process of our manuscript, a manuscript was published

477 uncovering the function of mammalian SETD3 in preventing primary dystocia and

478 presenting the structures of SETD3 bound to an unmodified actin peptide (66-80)

479 (Wilkinson et al., 2019). The structural findings reported in both manuscripts are

480 similar except that our complex structures contain a longer actin fragment (66-88) and

481   that the histidine is methylated in one of our complex.

482   **Materials and Methods**

Reagent type (species) or resource	Designation	Source or reference	Identifiers	Additional information
gene (*Escherichia coli*)	AdoHcy nucleosidase	NA	NCBI: NC_000913.3	
gene (*Bacillus subtilis*)	adenine deaminase	NA	NCBI: NC_000964.3	
gene (*H.sapiens*)	β-actin	NA	GenBank: NM_001101.4	
gene (*H.sapiens*)	SETD3	NA	NCBI: NM_032233.2	
recombinant DNA reagent	pCOLD I (plasmid)	Takara Bio	3361	
genetic reagent (E.coli)	pCOLD I/β-actin	PMID: 20851184		Kind gift of M. Tamura, Ehime University
genetic reagent (E.coli)	pCOLD I/SAH nucleosidase	PMID: 30526847		Overexpression of the recombinant *E.coli* AdoHcy nucleosidase in *E.coli* BL21 (DE3)
genetic reagent (E.coli)	pCOLD I/adenine deaminase	PMID: 30526847		Overexpression of the recombinant *B.subtilis* adenine deaminase in *E.coli* BL21 (DE3)
strain, strain background (*B.subtilis*)	*Bacillus subtilis*	Sigma-Aldrich	ATCC:6633	
strain, strain background (*E.coli*)	*E.coli* BL21 (DE3)	Agilent Technologies	200131	
chemical compound, drug	S-[methyl-^{3}H]adenosyl -L-methionine; [^{3}H]SAM	PerkinElmer	NET155V250UC; NET155V001MC	
software, algorithm	GraphPad Prism	GraphPad Software	RRID:SCR_002798	
pET28-MHL	vector	Addgene	26096 (Genbank accession number: EF456735)	Expression of SETD3 and its mutants
Origin 6.1, Origin 7.0	software	OriginLab	http://www.originlab.com/	For ITC curve fitting and calculation Kd values.
HKL2000	software	PMID: 27754618	http://www.hkl-xray.com/	Processing the crystal structure data
PHASER	software	PMID: 19461840	http://www.phaser.cimr.cam.ac.uk/	Molecular replacement
PHENIX	software	PMID: 20124702	http://www.phenix-online.org/	Structure refinement

Coot	software	PMID: 15572765	http://www2.mrc-lmb.cam.ac.uk/Personal/pemsley/coot/	Structure refinement
Pymol	software	DeLano Scientific LLC	http://www.pymol.org/	Making structure figures
MOLPROBITY	software	PMID: 20057044	http://molprobity.biochem.duke.edu/	Structure validation

483

Cloning, protein expression and purification of SETD3

Gene encoding the core region of SETD3 (2-502) were synthesized by Sangon Biotech (Shanghai) and cloned into pET28-MHL (Genbank accession number: EF456735). Then the plasmid was transformed into E. coli BL21 (DE3) and recombinant protein was over-expressed at 16 °C for 20 hours in the presence of 0.5 mM IPTG. Recombinant SETD3 proteins were purified by fast flow Ni-NTA column (GE Healthcare). N-terminal 6xHis-tag of recombinant proteins were removed by Tobacco Etch Virus (TEV) protease. Gel filtration and ion-exchange were employed for further purification. Purified SETD3 proteins, with their purities exceeding 90% as judged by SDS-PAGE, were concentrated to 15 mg/ml and stored at −80°C before further use. The SETD3 mutants were constructed by conventional PCR using the MutanBEST kit (TaKaRa) and further verified by DNA sequencing. The SETD3 mutants were expressed and purified in the same way as the wild type protein.

For kinetic studies, the enzyme and its mutant forms were produced as fusion proteins with the N-terminal 6xHis-tag and purified by Ni-NTA affinity chromatography. Briefly, the E. coli cell paste was resuspended in 11 ml lysis buffer consisting of 25 mM Hepes pH 7.5, 300 mM NaCl, 10 mM KCl, 1 mM DTT, 2 mM MgCl$_2$, 1 mM PMSF, 0.25 mg/ml hen egg white lysozyme (BioShop, Canada) and 250 U Viscolase (A and A Biotechnology, Poland). The cells were lysed by freezing in liquid nitrogen and, after thawing and vortexing, the extracts were centrifuged at 4° C (20000 x g for 20 min). For the purification, the supernatant of E. coli lysate (11 ml) was diluted 3-fold with buffer A (50 mM Tris-HCl pH 7.4, 400 mM NaCl, 10 mM KCl and 1 mM DTT) and applied onto a HisTrap FF crude column (1 ml) equilibrated with the 90%

508   buffer A and 10% buffer B (30 mM imidazole). The column was then washed with 12

509   ml 90% buffer A and 10% buffer B, and the retained proteins were eluted with a

510   stepwise gradient of imidazole (5 ml of 60 mM, 5 ml of 150 mM and 5 ml of 300

511   mM) in buffer A. The recombinant proteins eluted at the highest concentration of

512   imidazole was further processed. The enzyme preparation was desalted onto PD-10

513   columns equilibrated with 20 mM Tris-HCl pH 7.2, 50 mM KCl, 1 mM DTT and 6%

514   sucrose. The yield of recombinant proteins ranged from 1.6 mg to 0.1 mg for the

515   wild-type and N278A mutant, respectively, per 200 ml of culture. The purified

516   proteins were aliquoted and stored at –70°C.

517

518   **Overexpression and purification of the recombinant β-actin inclusion-body**

519   **protein**

520   Recombinant human β-actin (ACTB, GenBank: NM_001101.4) was prepared as

521   described before (Kwiatkowski et al., 2018). Plasmid pCOLD I that encodes   human

522   protein was a kind gift of Dr. Minoru Tamura (Ehime University, Japan) and was

523   prepared as described by (Tamura, 2018).

524

525   For β-actin production, Escherichia coli BL21(DE3) (Agilent, USA) cells were

526   transformed with the DNA construct and cultured in 500 mL of LB broth (with 100

527   μg/ml ampicilin) at 37 °C and 200 rpm until an OD_{600} of 0.5 was reached. Protein

528   production was induced by cold-shock (20 min on ice) and IPTG addition to a final

529   concentration of 0.2 mM. β-actin production was carried out for 20 h at 15 °C, 200

530   rpm, and harvested by centrifugation (6000 × g for 10 min). The cell paste was

531   resuspended in 27.5 ml lysis buffer consisted of 20 mM Hepes, pH 7.5, 1 mM DTT, 1

532   mM ADP, 0.5 mM PMSF, 2 μg/ml leupeptin and 2 μg/ml antipain, 0.2 mg/ml hen egg

533   white lysozyme (BioShop), 1000 U Viscolase (A&A Biotechnology, Poland). The

534   cells were lysed by freezing in liquid nitrogen and after thawing and vortexing, the

535   extracts were centrifuged at 4° C (20,000 × g for 30 min).

536

537   The pellet, containing inclusion bodies, was completely resuspended in buffer A (20

538 mM Hepes, pH 7.5, 2 M urea, 0.5 M NaCl, 5 mM DTT, 2 mM EDTA) with the use of

539 Potter-Elvehjem homogenizer and centrifuged at 4° C (20,000 × g for 10 min). The

540 resulting pellet was then subjected to a further two rounds of sequential wash in buffer

541 B (20 mM Hepes, pH 7.5, 0.5 M NaCl, 5 mM DTT, 2 mM EDTA) and buffer C (20

542 mM Hepes, pH 7.5, 0.5 M NaCl). The washed inclusion bodies were finally

543 solubilized in loading buffer (20 mM Tris-HCl, pH 7.5, 6 M guanidine HCl, 0.5 M

544 NaCl, 10 mM imidazole) and applied on a HisTrap FF column (5 ml) equilibrated

545 with the same buffer.

546

547 The column was washed with 20 ml of loading buffer and the bound protein was

548 refolded by the use of a linear gradient of 6-0 M guanidine HCl in loading buffer (40

549 ml for 20 min). Next, the column was washed with 15 ml of loading buffer without

550 guanidine HCl and the retained proteins were eluted with a stepwise gradient of

551 imidazole (25 ml of 40 mM, 25 ml of 60 mM and 20 ml of 500 mM). The

552 recombinant proteins were eluted with 500 mM imidazole in homogeneous form as

553 confirmed by SDS-PAGE (not shown). The β-actin preparation (10 ml) was

554 immediately dialyzed against 400 ml of the buffer consisted of 20 mM Tris-HCl, pH

555 7.5, 1 mM DTT, 6% sucrose, 2 μg/ml leupeptin and 2 μg/ml antipain. The dialysis

556 buffer was exchanged three times with the following dialysis time: 2, 2 and 12h. The

557 purified β-actin was stored at -70°C.

558

559 **Overexpression and purification of the recombinant SAH nucleosidase and**

560 **adenine deaminase**

561 *E. coli* DNA was extracted by heating 50 ml of over-night cultured BL21(DE3) cells

562 at 95°C for 15 min, whereas *Bacillus subtilis* (ATCC 6633, Sigma-Aldrich) genomic

563 DNA was purified from 100 mg of bacterial cells with the use of TriPure reagent

564 according to the manufacturer's instructions.

565

566 The open reading frames encoding *E. coli* SAH nucleosidase and *B. subtilis* adenine

567 deaminase (NCBI Reference Sequence: NC_000913.3 and NC_000964.3,

568 respectively) were PCR-amplified using either Pfu DNA polymerase alone or a

569 mixture of Taq:Pfu polymerases (1:0.2), respectively, in the presence of 1 M betaine.

570 SAH nucleosidase ORF was amplified using a 50 primer containing the initiator

571 codon preceded by an NdeI site and a 30 primer with a HindIII site, whereas adenine

572 deaminase DNA was amplified using a 50 primer with the initiator codon preceded by

573 an KpnI site and a 30 primer with a BamHI site (for primer sequences, see Table 5).

574 The amplified DNA products of expected size were digested with the appropriate

575 restriction enzymes, cloned into the pCOLD I expression vector (pCOLD I/SAH

576 nucleosidase and pCOLD I/adenine deaminase) and verified by DNA sequencing

577 (Macrogen, The Netherlands).

578

579 For protein production, *E. coli* BL21(DE3) cells were transformed with the

580 appropriate DNA construct and a single colony was selected to start an over-night

581 pre-culture. 100 mL of LB broth (with 100 mg/mL ampicilin) was inoculated with 10

582 ml of the pre-culture and incubated at 37°C and 200 rpm until an OD600 of 0.6 was

583 reached. The culture was placed on ice for 20 min (cold-shock) and IPTG was added

584 to a final concentration of 0.25 mM to induce protein expression. Cells were

585 incubated for 16 hr at 13°C, 200 rpm, and harvested by centrifugation (6000 x g for

586 10 min). The cel pellet was resuspended in 10 ml lysis buffer consisting of 25 mM

587 Hepes pH 7.5, 300 mM NaCl, 50 mM KCl, 1 mM DTT, 2 mM MgCl2, 1 mM PMSF,

588 5 mg/ml leupeptin and 5 mg/ml antipain, together with 0.25 mg/ml hen egg white

589 lysozyme (BioShop) and 25 U DNase I (Roche). The cells were lysed by freezing in

590 liquid nitrogen and, after thawing and vortexing, the extracts were centrifuged at 4°C

591 (20,000 x g for 30 min).

592 For protein purification, the supernatant of the *E. coli* lysate (10 ml) was diluted

593 3-fold with buffer A (50 mM Tris-HCl, pH 7.2, 400 mM NaCl, 10 mM KCl, 30 mM

594 imidazole, 1 mM DTT, 3 mg/ml leupeptin and 3 mg/ml antipain) and applied onto a

595 HisTrap FF column (5 ml) equilibrated with the same buffer. The column was washed

596 with 20–30 ml buffer A and the retained protein was eluted with a stepwise gradient

597 of imidazole (25 ml of 60 mM, 20 ml of 150 mM and 20 ml of 300 mM) in buffer A.

598   The recombinant proteins were eluted with 150–300 mM imidazole in homogeneous

599   form, as confirmed by SDS-PAGE (not shown). The enzyme preparations were

600   desalted onto PD-10 columns equilibrated with 20 mM Tris-HCl pH 7.2, 50 mM KCl,

601   1 mM DTT, 6% sucrose, 2 mg/ml leupeptin and 2 mg/ml antipain. The yield of

602   recombinant proteins was 1.2 mg and 3.1 mg of homogenous adenine deaminase and

603   SAH nucleosidase, respectively, per 200 ml of *E. coli* culture. The purified enzymes

604   were aliquoted and stored at –70°C.

605

606   **Isothermal titration calorimetry (ITC)**

607   All peptides were synthesized by GL Biochem (Shanghai) Ltd. and were dissolved in

608   water as a stock of 5-12 mM, with the pH of stock solutions adjusted to pH 7.5.

609   Peptides and concentrated proteins were diluted with ITC buffer (20 mM Tris, pH 7.5

610   and 150 mM NaCl). ITC experiments were performed by titrating 2 μl of peptide

611   (1.2-1.5 mM) into cell containing 50 μM proteins on MicroCal™ (Malvern

612   Panalytical, UK) at 25°C, with a spacing time of 160 s and a reference power of 10

613   μCal/s. Control experiments were performed by injection of peptides into buffer.

614   Binding isotherms were plotted, analyzed and fitted in a one-site binding model by

615   MicroCal PEAQ-ITC Analysis Software (Malvern Panalytical, UK) after subtraction

616   of respective controls. The dissociation constants (Kds) were from a minimum of two

617   experiments (mean ± sd). The ITC binding curves are shown in Supplemental File 1.

618

619   **Crystallization, data collection and structure determination**

620   All crystals were grown by using sitting drop vapor diffusion method at 18°C. For

621   crystallization of SETD3 with methylated peptide, SETD3 (12 mg/ml) was

622   pre-incubated with synthesized β-actin peptide (66-88) (GL Biochem Ltd.) and

623   AdoMet at a molar ratio of 1:3:4, and mixed with the crystallization buffer containing

624   0.1 M sodium cacodylate trihydrate pH 6.5, 0.2M magnesium acetate tetrahydrate,

625   and 20% v/v polyethylene glycol 8000. For the crystallization of SETD3 with

626   unmodified peptide, SETD3, in the concentration of 12 mg/ml, was pre-incubated

627   with synthesized β-actin peptide (66-88) and AdoHcy at a molar ratio of 1:3:4, and

628   mixed with the crystallization buffer containing 0.1M HEPES sodium pH 7.5, 2% v/v

629   polyethylene glycol 400, and 2.0 M ammonium sulfate. Before flash-freezing crystals

630   in liquid nitrogen, all crystals were soaked in a cryo-protectant consisting of 90%

631   reservoir solution plus 10% glycerol. The diffraction data were collected on BL17U1

632   at the Shanghai Synchrotron Facility (Wang et al., 2016) (SSRF). Data sets were

633   collected at 0.9789 Å or 0.9789 Å, and were processed by using the HKL2000

634   program (Otwinowski and Minor, 1997).

635

636   The initial structures of the SETD3-actin complexes were solved by molecular

637   replacement using Phaser (McCoy et al., 2007) with previously solved SETD3

638   structure (PDB: 3SMT) as the search model. Then all the models were refined

639   manually and built with Coot (Emsley and Cowtan, 2004). The final structures were

640   further refined by PHENIX (Adams et al., 2010). The statistics for data collection and

641   refinement are summarized in Table 2.

642

643   **Mass Spectrometry**

644   Reversed-phase microcapillary/tandem mass spectrometry (LC/MS/MS) was

645   performed using an Easy-nLC nanoflow HPLC (Proxeon Biosciences) with a

646   self-packed 75 μm id x 15 cm C18 column connected to either an QE-Plus (Thermo

647   Scientific) in the data-dependent acquisition and positive ion mode at 300 nL/min.

648   Passing MS/MS spectra were manually inspected to be sure that all b- and y- fragment

649   ions aligned with the assigned sequence and modification sites. A 25-ul reaction

650   mixture containing 2 μM SETD3 or SETD3 mutants (final concentration), 20 μM

651   peptide (final concentration) in a buffer containing 10 mM Tris-HCl, pH 7.5, 20 mM

652   NaCl and 10 μM AdoMet. The reaction was incubated at 37℃ for 2h before being

653   quenched (at 70℃ for 10-15 mins). Then reactions were analyzed by LC/MS/MS and

654   Proteomics Browser Software, with the relative abundances of substrate and product

655   reflecting the methylation activities of proteins.

656

657   **Radiochemical Assay of the SETD3 Activity**

658   The enzyme activity was determined by measuring the incorporation of [^{3}H]methyl

659   group from S-[methyl-^{3}H]adenosyl-L-methionine ([^{3}H]AdoMet) into homogenous

660   recombinant human (mammalian) β-actin or its mutated form in which histidine 73

661   was replaced by alanine residue (H73A). The standard incubation mixture (0.06-0.11

662   ml) contained 25 mM Tris-HCl, pH 7.2, 10 mM KCl, 1 mM DTT and various

663   concentration of protein substrate and [^{1}H+^{3}H] AdoMet ($\approx$ 300-700 $\times$ 10^3 cpm) as

664   indicated in legends to figures and tables. The incubation mixture was supplemented

665   with recombinant AdoHcy nucleosidase and adenine deaminase to prevent AdoHcy

666   accumulation as indicated in legends to figures and tables. The reaction was started by

667   the addition of enzyme preparation and carried out at 37°C for 10 min. Protein

668   methylation was linear for at least 15 min under all conditions studied. By analogy to

669   assays of nonribosomal peptide synthetase activity (Richardt et al., 2003; Drozak et

670   al., 2014), the incubation was stopped by the addition of 0.05-0.11 ml of the reaction

671   mixture to 0.025 ml of BSA (1 mg) and 0.8 ml of ice-cold 10 % (w/v) trichloroacetic

672   acid (TCA). After 10 min on ice, the precipitate was pelleted and washed twice with

673   ice-cold 10 % TCA. The pellet was finally dissolved in pure formic acid.

674

675   **Calculations**

676   V_{max}, K_M and k_{cat} for the methyltransferase activity of the studied enzymes were

677   calculated with Prism 8.0 (GraphPad Software, La Jolla, USA) using a nonlinear

678   regression.

679

680   **ACCESSION NUMBERS**

681   The coordinates and structure factors of AdoHcy bound SETD3 with unmodified

682   β-actin peptide and methylated β-actin peptide haven been deposited into Protein Data

683   Bank (PDB) with accession numbers 6ICV and 6ICT, respectively.

684

685   **SUPPLEMENTARY INFORMATION**

686   Supplemental File can be found online at XXXX

687

CONFLICT OF INTEREST

The authors declare that they have no conflict of interest related to the publication of this manuscript.

REFERENCES

Adams, P.D., Afonine, P.V., Bunkoczi, G., Chen, V.B., Davis, I.W., Echols, N., Headd, J.J., Hung, L.W.,

718   Kapral, G.J., Grosse-Kunstleve, R.W*., et al.* (2010). PHENIX: a comprehensive Python-based system for
719   macromolecular structure solution. Acta crystallographica Section D, Biological crystallography *66*,
720   213-221.
721   Cao, R., Zhang, X., Liu, X., Li, Y., and Li, H. (2018). Molecular basis for histidine N1 position-specific
722   methylation by CARNMT1. Cell Res *28*, 494-496.
723   Chang, Y., Levy, D., Horton, J.R., Peng, J., Zhang, X., Gozani, O., and Cheng, X. (2011). Structural basis of
724   SETD6-mediated regulation of the NF-kB network via methyl-lysine signaling. Nucleic Acids Res *39*,
725   6380-6389.
726   Cheng, X., Hao, Y., Shu, W., Zhao, M., Zhao, C., Wu, Y., Peng, X., Yao, P., Xiao, D., Qing, G*., et al.* (2017).
727   Cell cycle-dependent degradation of the methyltransferase SETD3 attenuates cell proliferation and
728   liver tumorigenesis. The Journal of biological chemistry *292*, 9022-9033.
729   Dillon, S.C., Zhang, X., Trievel, R.C., and Cheng, X. (2005). The SET-domain protein superfamily: protein
730   lysine methyltransferases. Genome biology *6*, 227.
731   dos Remedios, C.G., Chhabra, D., Kekic, M., Dedova, I.V., Tsubakihara, M., Berry, D.A., and Nosworthy,
732   N.J. (2003). Actin binding proteins: regulation of cytoskeletal microfilaments. Physiol Rev *83*, 433-473.
733   Drozak, J., Piecuch, M., Poleszak, O., Kozlowski, P., Chrobok, L., Baelde, H.J., and de Heer, E. (2015).
734   UPF0586 Protein C9orf41 Homolog Is Anserine-producing Methyltransferase. The Journal of biological
735   chemistry *290*, 17190-17205.
736   Emsley, P., and Cowtan, K. (2004). Coot: model-building tools for molecular graphics. Acta
737   crystallographica Section D, Biological crystallography *60*, 2126-2132.
738   Eom, G.H., Kim, K.B., Kim, J.H., Kim, J.Y., Kim, J.R., Kee, H.J., Kim, D.W., Choe, N., Park, H.J., Son, H.J*., et*
739   *al.* (2011). Histone methyltransferase SETD3 regulates muscle differentiation. The Journal of biological
740   chemistry *286*, 34733-34742.
741   Gunning, P., Ponte, P., Okayama, H., Engel, J., Blau, H., and Kedes, L. (1983). Isolation and
742   characterization of full-length cDNA clones for human alpha-, beta-, and gamma-actin mRNAs: skeletal
743   but not cytoplasmic actins have an amino-terminal cysteine that is subsequently removed. Mol Cell
744   Biol *3*, 787-795.
745   Herman, I.M. (1993). Actin isoforms. Curr Opin Cell Biol *5*, 48-55.
746   Holm, L., and Rosenstrom, P. (2010). Dali server: conservation mapping in 3D. Nucleic Acids Res *38*,
747   W545-549.
748   Johnson, P., Harris, C.I., and Perry, S.V. (1967). 3-methylhistidine in actin and other muscle proteins.
749   Biochem J *105*, 361-370.
750   Kabsch, W., Mannherz, H.G., Suck, D., Pai, E.F., and Holmes, K.C. (1990). Atomic structure of the
751   actin:DNase I complex. Nature *347*, 37-44.
752   Kwiatkowski, S., Seliga, A.K., Vertommen, D., Terreri, M., Ishikawa, T., Grabowska, I., Tiebe, M.,
753   Teleman, A.A., Jagielski, A.K., Veiga-da-Cunha, M*., et al.* (2018). SETD3 protein is the actin-specific
754   histidine N-methyltransferase. Elife *7*.
755   Leterrier, C., Dubey, P., and Roy, S. (2017). The nano-architecture of the axonal cytoskeleton. Nat Rev
756   Neurosci *18*, 713-726.
757   Malecki, J., Aileni, V.K., Ho, A.Y.Y., Schwarz, J., Moen, A., Sorensen, V., Nilges, B.S., Jakobsson, M.E.,
758   Leidel, S.A., and Falnes, P.O. (2017). The novel lysine specific methyltransferase METTL21B affects
759   mRNA translation through inducible and dynamic methylation of Lys-165 in human eukaryotic
760   elongation factor 1 alpha (eEF1A). Nucleic Acids Res *45*, 4370-4389.
761   McCoy, A.J., Grosse-Kunstleve, R.W., Adams, P.D., Winn, M.D., Storoni, L.C., and Read, R.J. (2007).

762 Phaser crystallographic software. Journal of applied crystallography *40*, 658-674.

763 Min, J., Feng, Q., Li, Z., Zhang, Y., and Xu, R.M. (2003). Structure of the catalytic domain of human
764 DOT1L, a non-SET domain nucleosomal histone methyltransferase. Cell *112*, 711-723.

765 Nudel, U., Zakut, R., Shani, M., Neuman, S., Levy, Z., and Yaffe, D. (1983). The nucleotide sequence of
766 the rat cytoplasmic beta-actin gene. Nucleic Acids Res *11*, 1759-1771.

767 Nyman, T., Schuler, H., Korenbaum, E., Schutt, C.E., Karlsson, R., and Lindberg, U. (2002). The role of
768 MeH73 in actin polymerization and ATP hydrolysis. J Mol Biol *317*, 577-589.

769 Otwinowski, Z., and Minor, W. (1997). Processing of X-ray diffraction data collected in oscillation mode.
770 Methods in enzymology *276*, 307-326.

771 Perrin, B.J., and Ervasti, J.M. (2010). The actin gene family: function follows isoform. Cytoskeleton
772 (Hoboken) *67*, 630-634.

773 Raghavan, M., Lindberg, U., and Schutt, C. (1992). The use of alternative substrates in the
774 characterization of actin-methylating and carnosine-methylating enzymes. Eur J Biochem *210*,
775 311-318.

776 Rhein, V.F., Carroll, J., Ding, S., Fearnley, I.M., and Walker, J.E. (2017). Human METTL12 is a
777 mitochondrial methyltransferase that modifies citrate synthase. FEBS Lett *591*, 1641-1652.

778 Tamura, M. (2018). Production of Human beta-Actin Using a Bacterial Expression System with a Cold
779 Shock Vector. Curr Protoc Protein Sci *93*, e61.

780 Terman, J.R., and Kashina, A. (2013). Post-translational modification and regulation of actin. Curr Opin
781 Cell Biol *25*, 30-38.

782 Theriot, J.A., and Mitchison, T.J. (1991). Actin microfilament dynamics in locomoting cells. Nature *352*,
783 126-131.

784 Trievel, R.C., Beach, B.M., Dirk, L.M., Houtz, R.L., and Hurley, J.H. (2002). Structure and catalytic
785 mechanism of a SET domain protein methyltransferase. Cell *111*, 91-103.

786 Vijayasarathy, C., and Rao, B.S. (1987). Partial purification and characterisation of
787 S-adenosylmethionine:protein-histidine N-methyltransferase from rabbit skeletal muscle. Biochim
788 Biophys Acta *923*, 156-165.

789 Wagner, E.J., and Carpenter, P.B. (2012). Understanding the language of Lys36 methylation at histone
790 H3. Nat Rev Mol Cell Biol *13*, 115-126.

791 Wang, Z., Pan, Q., Yang, L., Zhou, H., Xu, C., Yu, F., Wang, Q., Huang, S., and He, J. (2016). Automatic
792 crystal centring procedure at the SSRF macromolecular crystallography beamline. Journal of
793 synchrotron radiation *23*, 1323-1332.

794 Webb, K.J., Zurita-Lopez, C.I., Al-Hadid, Q., Laganowsky, A., Young, B.D., Lipson, R.S., Souda, P., Faull,
795 K.F., Whitelegge, J.P., and Clarke, S.G. (2010). A novel 3-methylhistidine modification of yeast
796 ribosomal protein Rpl3 is dependent upon the YIL110W methyltransferase. The Journal of biological
797 chemistry *285*, 37598-37606.

798 Wilkinson, A.W., Diep, J., Dai, S., Liu, S., Ooi, Y.S., Song, D., Li, T.M., Horton, J.R., Zhang, X., Liu, C., *et al.*
799 (2019). SETD3 is an actin histidine methyltransferase that prevents primary dystocia. Nature *565*,
800 372-376.

801 Xu, C., Ishikawa, H., Izumikawa, K., Li, L., He, H., Nobe, Y., Yamauchi, Y., Shahjee, H.M., Wu, X.H., Yu, Y.T.,
802 *et al.* (2016). Structural insights into Gemin5-guided selection of pre-snRNAs for snRNP assembly.
803 Genes Dev *30*, 2376-2390.

804

805

TABLES

Table 1. Binding affinities of SETD3 proteins to β-actin peptides

Table 2. Data collection and refinement statistics

Table 3. Kinetic properties of wild type SETD3 and its mutants.

FIGURES LEGENDS

Figure 1. SETD3 core region specifically recognizes a fragment of β-actin containing His73. (A) Domain architecture of full-length human SETD3 (aa 1-594) and the sequence of the β-actin peptide (66-88), with His73 of β-actin highlighted. (B) Representative ITC binding curves for the binding of the SETD3 (aa 2-502) to β-actin peptides of different lengths. Molecular ratios, derived Kds and respective standard deviations are also indicated. (C) Overall structure of AdoHcy bound SETD3 with unmodified β-actin peptide. The SETD3 are colored in the same mode as shown in Figure 1a, with the N-SET, SET, iSET and C-SET regions of SETD3 colored in grey, blue, purple and salmon, respectively. The peptide are shown in yellow cartoon, while His73 and AdoHcy are shown in yellow and cyan sticks, respectively. His73 of actin and the AdoHcy are labeled.

Figure 2. Molecular mechanism of substrate recognition and histidine methylation by SETD3. (A) The β-actin peptide is bound in a long groove on the surface of SETD3 N-lobe region (right), with His73 of β-actin positioned into a hydrophobic pocket (left). His73 and AdoHcy are shown in yellow and cyan sticks, respectively, and their 2|Fo|–|Fc| σ-weighted maps are contoured at 1.2 σ. His73 binding residues of SETD3 are colored based on the regions that they reside as shown in Figure 1A. (B) Detailed interactions between His73me and SETD3 in the post-methyl transfer complex. His73me and AdoHcy are shown in yellow and cyan sticks, respectively, and their 2|Fo|–|Fc| σ-weighted maps are contoured at 1.2 σ. His73me binding residues of SETD3 are colored in the same mode as shown in Figure 2A. (C) Superposition of the two complexes on the histidine/methylhistidine binding pocket. For the SETD3-His73me complex, His73me binding residues of SETD3 are

836   shown in the same way as in Figure 2A, with His73me and AdoHcy shown in yellow

837   and cyan sticks, respectively. For the SETD3-His73 complex, His73 binding residues

838   and AdoHcy are shown in grey sticks, while His73 are shown in green sticks to show

839   that it rotates 90 degree after catalysis. After methylation, one new hydrogen bond is

840   formed between Asn256 and N^1 atom of His73me (red dash). (D) lysine recognition

841   by LSMT(PDB id: 1OZV) in the presence of AdoHcy. (E) carnosine recognition by

842   CARNMT1 (PDB id: 5YF1) in the presence of SFG. Histidine, lysine and carnosine

843   are shown in yellow sticks, while the protein residues involved in binding are shown

844   in red sticks. AdoHcy and its mimic, SFG, are shown in cyan sticks.

845

846   **Figure 3. Effect of pH on SETD3 enzyme activity.**

847   pH dependence of human SETD3 was determined with the use of purified

848   recombinant N-terminal His6-tagged SETD3 protein (2-502). The enzyme preparation

849   (0.045 μg protein) was incubated at 37°C for 10 min in the presence of 0.8 μM

850   $[^1H+^3H]$ AdoMet (80 pmol, ≈350 × 10^3 cpm) and either 5 μM (500 pmol, 22.34 μg)

851   purified recombinant human β-actin or its mutated form (H73A) which served as a

852   negative control. In all experiments, the reaction mixture contained the homogenous

853   recombinant AdoHcy nucleosidase (1.6 mg protein, 600 nM, E. coli) and adenine

854   deaminase (3.9 mg protein, 600 nM, B. subtilis) to prevent AdoHcy accumulation.

855   The reaction was stopped and the proteins present in the assay mixture were

856   precipitated by adding 10% trichloroacetic acid. This allowed for the separation and

857   specific measurement of the radioactivity incorporated in the protein pellet (extent of

858   actin methylation) from the total radioactivity present in the assay mixture. Values are

859   the means ± S.E. (error bars) of three separate experiments. If no an error bar is

860   visible, it is shorter than the size of the symbol.

861

862   **FIGURE SUPPLEMENTS**

863   **Figure 1 - figure supplement 1. Mass Spectrometry data showing the activity of**

864   **SETD3 towards different peptides.** Core region of SETD3 (2-502) methylates (A)

865   the β-actin peptide (aa 66-88), but not (B) H3K4 (1-23), (C) H3K36 (25-47), or (D)

866   β-actin H73A(66-88) (E) The activity of SETD3 mutants on the β-actin peptide

867   (66-88).

868   **Figure 1 - figure supplement 2. Sequence alignment of human SETD3 with its**

869   **orthologs or other SET domain proteins (SETD6 and LSMT).** (A) Sequence

870   alignment of Human SETD3(Hs, NP_115609.2), mouse SETD3(Ms, NP_082538.2),

871   Xenopus SETD3(Xs, NP_001016577), Zebrafish SETD3 (Zb, NP_956348.1) and

872   Drosophila (Dr, XP_017048262.1). The secondary structures of human SETD3 are

873   colored in the same way as shown in Figure 1A. The residues involved in binding to

874   AdoHcy and His73 are labeled in cyan and yellow, respectively. (B) Sequence

875   aligment of human SETD3, human SETD6 (NP_001153777.1) and Pisum sativum

876   LSMT (AAA69903.1). The secondary structures, AdoHcy binding residues, and

877   His73 binding residues, are labeled in the same way as shown in Figure 1–figure

878   supplement 2A.

879   **Figure 1 - figure supplement 3. Topology of SETD3 (2-502)**, with secondary

880   structures marked and colored in the same way as shown in Figure 1–figure

881   supplement 2A.

882   **Figure 1 - figure supplement 4. Superposition of SETD3 molecules.** (A)

883   Superposition of four SETD3 molecules bound to methylated β-actin in the same

884   asymmetric unit, with the four molecules shown in red, green, blue and yellow ribbon,

885   respectively. His73me of β-actin and AdoHcy are shown in sticks. (B) Superposition

886   of two molecules of SETD3 bound to unmodified β-actin in the same asymmetric unit,

887   with the two molecules shown in red and green ribbon, respectively. His73 of β-actin

888   and AdoHcy are shown in sticks.

889   **Figure 1 - figure supplement 5. The 2|Fo|–|Fc| σ-weighted maps of (A) methylated**

890   **β-actin peptide and (B) unmodified β-actin peptide in the presence of AdoHcy**,

891   are contoured at 1.2 σ (blue cage), respectively. The peptides are shown in yellow

892   sticks.

893   **Figure 1 - figure supplement 6. Comparison of AdoHcy binding mode of**

894   **SETD3 with those observed in LSMT and SETD6.** (A) A detailed depiction of

895   intermolecular interactions between SETD3 and AdoHcy, with AdoHcy shown in

896   cyan sticks, and the AdoHcy binding residues of SETD3 shown in sticks and colored

897   in the same mode as in Figure 1A. (B) Detailed interactions between AdoHcy and

898   LSMT (PDB id: 1MLV), with AdoHcy binding residues of LSMT and AdoHcy shown

899   in green and cyan sticks, respectively. (C) Detailed interactions between AdoMet and

900   SETD6 (PDB id: 3QXY), with AdoMet binding residues of SETD6 and AdoMet

901   shown in orange and cyan sticks, respectively. In Figures 2B and 2C, hydrogen bonds

902   are indicated by black dashes.

903   **Figure 1 - figure supplement 7. Superposition of AdoMet-bound SETD3 (PDB**

904   **id: 3SMT) with AdoHcy bound SETD3-actin.** In the structure of AdoMet bound

905   SETD3, the protein is shown in grey ribbon and AdoMet is shown in grey sticks. In

906   the structure of AdeHcy bound SETD3 in the presence of actin, protein is shown in

907   blue ribbon and AdoHcy is shown in yellow sticks. β4-β9-β10 and β3-β11 changed

908   conformations significantly upon binding to actin peptide, which are shown in cartoon

909   representation. Leu67-Ile71 of β-actin and their interaction residues in SETD3, are

910   shown in sticks. Three loops that precede β4, β9 and β11 shift 4.2Å, 4.4Å, and 6.8Å,

911   respectively.

912   **Figure 1 - figure supplement 8. Overall structure of SETD3 with methylated**

913   **β-actin peptide in the presence of AdoHcy.** SETD3 is colored and labelled in the

914   same mode as shown in Figure 1C. AdoHcy and His73me are shown in sticks.

915   **Figure 2 - figure supplement 1. Detailed interactions of SETD3 and β-actin**

916   **peptide (66-88).** The β-actin peptide mainly contacts N-terminal lobe of SETD3, with

917   its N-terminal and C-terminal sides contact SET and iSET domains, respectively. In

918   the top panel, SETD3 are shown in ribbon and colored in the same way as shown in

919   Figure 2A. β-actin peptide is shown in yellow sticks. Detailed interactions between

920   SETD3 and Leu67-Glu72, and between SETD3 and Gly74 and Glu83, are shown in

921   the left bottom and right bottom panels, respectively. The SETD3 residues involved in

922   β-actin binding are shown in sticks.

923   **Figure 2 - figure supplement 2. Schematic of the detailed interactions (A)**

924   **between SETD3 and unmodified β-actin (B) and between SETD3 and methylated**

925   **β-actin.** SETD3 residues are colored as shown in Figure 1A, while the peptide

926 residues are colored in yellow. The hydrophobic interactions and hydrogen bonds

927 between protein and peptide are shown in black solid arrows and black dash arrows,

928 respectively.

929 **Figure 2 - figure supplement 3. Actin endures conformational changes upon**

930 **binding to SETD3.** β-actin peptide (66-88, yellow cartoon) is over laid with the same

931 fragment in the structure of native β-actin (red cartoon) (PDB id: 1HLU). native

932 β-actin decomposes its local   secondary structures upon SETD3 binding.   Native

933 β-actin and SETD3 are shown in red and blue ribbon, respectively.

934

935 **Suppplemental File 1.** ITC binding curves for the binding measurements reported in

936 Table 1.

937

938 **TITLES FOR THE SOURCE DATA FILES**

939 **Figure 3 – Source Data 1.** Radiochemical measurements of SETD3-dependent

940 methylation of either human recombinant β-actin or its mutated form (H73A) in the

941 presence of increasing pH value of the reaction mixture.

942 **Table 3 – Source Data 1**. Determination of kinetic parameters of SETD3-catalyzed

943 methylation of actin (for β-actin as the substrate).

944 **Table 3 – Source Data 2.** Determination of kinetic parameters of SETD3-catalyzed

945 methylation of actin (for AdoMet as the substrate).

Table 1. Binding affinities of SETD3 proteins to β-actin peptides.

β-actin Peptide	SETD3 (2-502)	Stoichiometric coefficient (N)	Kd (μM)
[66]TLKYPIEHGIVTNWDDMEKIWHH[88]	Wild type	1.0	0.17 ± 0.04
[66]TLKYPIEAGIVTNWDDMEKIWHH[88] (H73A)	Wild type	1.3	0.45 ± 0.08
[1]ARTKQTARKSTGGKAPRKQLATK[23] (H3K4)	Wild type	#N/A	*NB
[25]ARKSAPATGGVKKPHRYRPGTVA[47] (H3K36)	Wild type	N/A	NB
[66]TLKYPIEHGIVTNWDDMEKIWHH[88]	R215A	1.2	3.6 ± 1.0
[66]TLKYPIEHGIVTNWDDMEKIWHH[88]	N256A	0.94	2.1 ± 0.4
[66]TLKYPIEHGIVTNWDDMEKIWHH[88]	N256D	1.3	23 ± 7
[66]TLKYPIEHGIVTNWDDMEKIWHH[88]	N256Q	1.1	2.5 ± 0.5
[66]TLKYPIEHGIVTNWDDMEKIWHH[88]	W274A	0.94	0.51 ± 0.10
[66]TLKYPIEHGIVTNWDDMEKIWHH[88]	Y313F	0.86	3.0 ± 0.1
[66]TLKYPIEHGIVTNWDDMEKIWHH[88]	R316A	1.1	7.4 ± 0.9
[66]TLKAPIEHGIVTNWDDMEKIWHH[88] (Y69A)	Wild type	1.4	3.8 ± 0.8
[66]TLKYPAEHGIVTNWDDMEKIWHH[88] (I71A)	Wild type	1.3	16 ± 3
[66]TLKYPIEHGIVTNWADMEKIWHH[88] (D80A)	Wild type	1.3	3.5 ± 0.4
[66]TLKYPIEHGIVTNWDAMEKIWHH[88] (D81A)	Wild type	1.3	2.0 ± 0.5
[66]TLKYPIEHGIVTNWDDAEKIWHH[88] (M82A)	Wild type	1.2	0.89 ± 0.08
[66]TLKYPIEHGIVTNWD[80]	Wild type	1.0	2.9 ± 0.7

#N/A: Not applicable; *NB: No detectable binding affinity by ITC.

Dissociation constants (Kds) were from a minimum of two experiments (mean ± sd). The original binding curves are shown in Supplemental file 1.

49 **Table 2. Data collection and refinement statistics**

50

	SETD3-β-actin	SETD3-methylated β-actin
PDB id	6ICV	6ICT
Data collection		
Radiation wavelength (Å)	0.9789	0.9792
Space group	P 1 21 1	P 1 21 1
Cell dimensions		
a, *b*, *c* (Å)	60.19, 175.17, 66.50	59.98,176.69,125.89
α, β, γ (°)	90, 92.57, 90	90,93.37,90
Resolution (Å)	35.00-2.15(2.23-2.15)	72.27-1.95(2.06-1.95)
R_{merge}	0.135(0.609)	0.169(0.868)
I / σ*I*	14(3.4)	8.1(2.6)
CC1/2	0.988(0.884)	0.991(0.827)
Completeness (%)	100(100)	99.1(99.7)
Redundancy	6.4(6.4)	7.0(7.0)
Refinement		
Resolution (Å)	35.00-2.15	59.87-1.95
No. of reflections (used/free)	71998/3629	187163/9084
R_{work}/R_{free}	0.168/0.205	0.178/0.214
Number of atoms/B-factor ($Å^2$)	8493/30.7	16956/33.7
Protein	7574/30.3	15147/33.1
Peptide	276/32.9	591/38.4
AdoHcy	52/19.3	104/20.0
Solvent	591/36.2	1114/40.0
RMSD bonds (Å)/angles (°)	0.007/0.84	0.007/0.87
Ramachandran Plot		
favored/allowed/outliers (%)	98.76/1.24/0	98.98/1.02/0

51 Values in parentheses are for highest-resolution shell.

52

53

54

55

56

57

58

59

60

61

62

63

64

65

66

67

68

69

70

71 **Table 3. Kinetic properties of wild type SETD3 and its mutants.**

72 Kinetic parameters were determined with the use of purified recombinant N-terminal His$_6$-tagged SETD3

73 proteins.

74

SETD3	Substrate	Kinetic Parameters			
		V_{max}	K_M	k_{cat}	k_{cat}/K_M
		$nmol\ min^{-1}\ mg^{-1}$	μM	min^{-1}	$min^{-1}\ \mu M^{-1}$
Wild type	β-actin	13.550±0.364	0.502±0.041	0.809	1.612
R75A		0.037±0.002	0.565±0.071	0.002	0.004
R215A		3.553±0.068	1.087±0.056	0.212	0.195
N256A		0.512±0.019	0.449±0.053	0.031	0.069
N256D		0.973±0.017	0.305±0.0196	0.058	0.190
N256Q		10.860±0.172	0.784±0.035	0.649	0.828
N278A		0.019±0.000	0.047±0.009	0.001	0.021
Y313F		0.367±0.005	0.581±0.023	0.022	0.038
R316A		2.903±0.0477	1.115±0.049	0.173	0.155
Wild type	AdoMet	11.260±0.466	0.111±0.020	0.673	6.063
R75A		0.265±0.072	3.601±1.363	0.016	0.004
R215A		3.666±0.078	0.165±0.013	0.219	1.327
N256A		1.136±0.038	0.686±0.052	0.068	0.099
N256D		0.671±0.021	0.165±0.019	0.040	0.242
N256Q		6.368±0.266	0.103±0.019	0.380	3.689
N278A		0.018±0.001	0.350±0.042	0.001	0.003
Y313F		1.623±0.348	6.543±1.736	0.097	0.015
R316A		4.099±0.054	0.149±0.008	0.244	1.638

75

76 Determinations for *S*-adenosyl-L-methionine (AdoMet) were performed with the SETD3 preparations (0.05-5.00 μg

77 protein, 8.38-838 nM) that were incubated for 10 min at 37°C in the reaction mixture containing 5 μM recombinant

78 human β-actin and variable concentrations of [^{1}H+^{3}H] SAM (≈330 × 10^3 cpm), while the measurements for β-actin were

79 done following a 10-min incubation of SETD3 in the presence of 0.8 μM concentration of [^{1}H+^{3}H] SAM (80 pmol,

80 300-700 × 10^3 cpm). In all experiments reaction mixture contained the homogenous recombinant SAH nucleosidase (1.6

81 μg protein, 600 nM, *E. coli*) and adenine deaminase (3.9 μg protein, 600 nM, *B. subtilis*) to prevent

82 *S*-adenosyl-L-homocysteine (AdoHcy) accumulation. Values are the means of three separate experiments. The S.E.
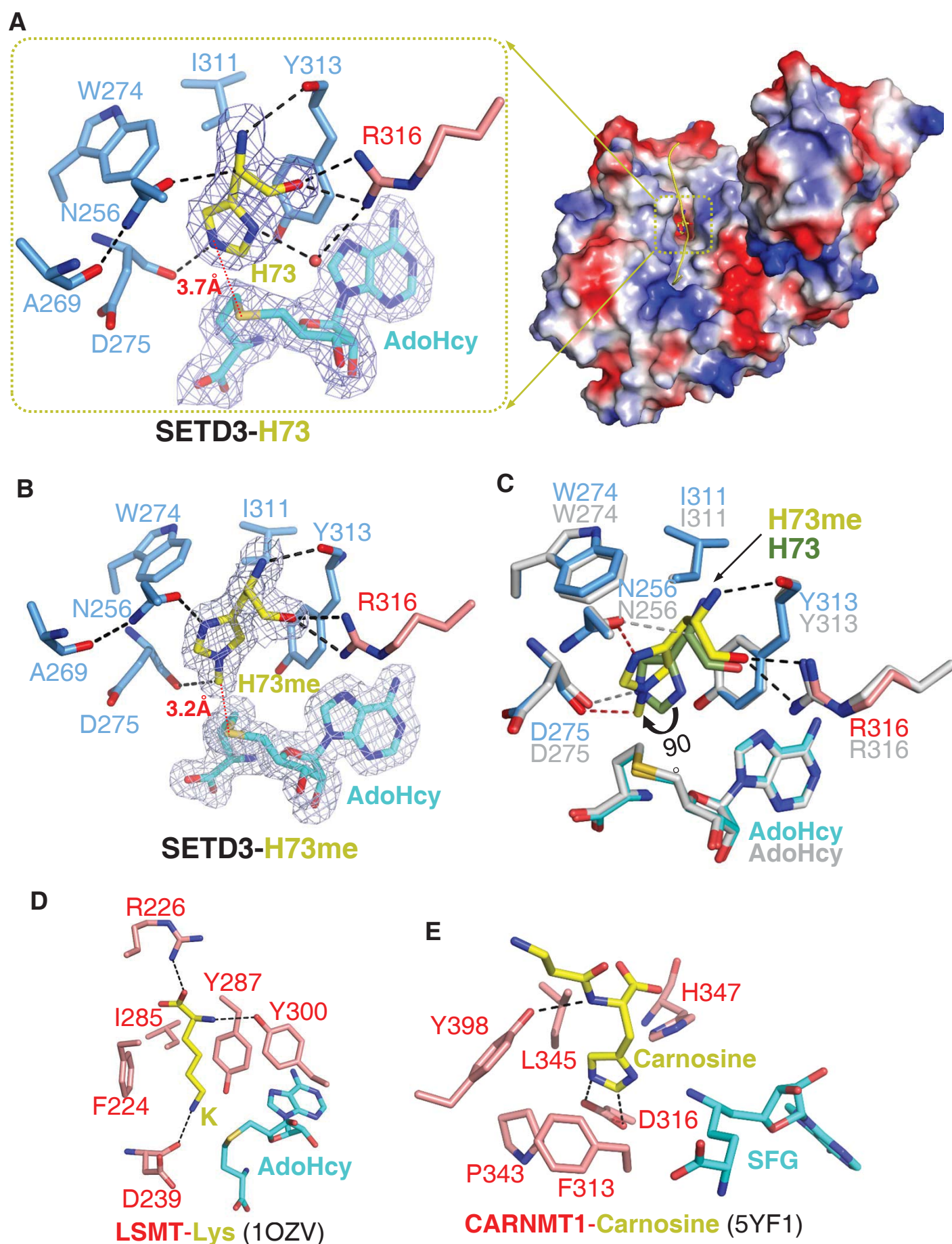
83 values are also given.

Figure 1

Figure 3

A

SETD3-H73

B

SETD3-H73me

C

D

LSMT-Lys (1OZV)

E

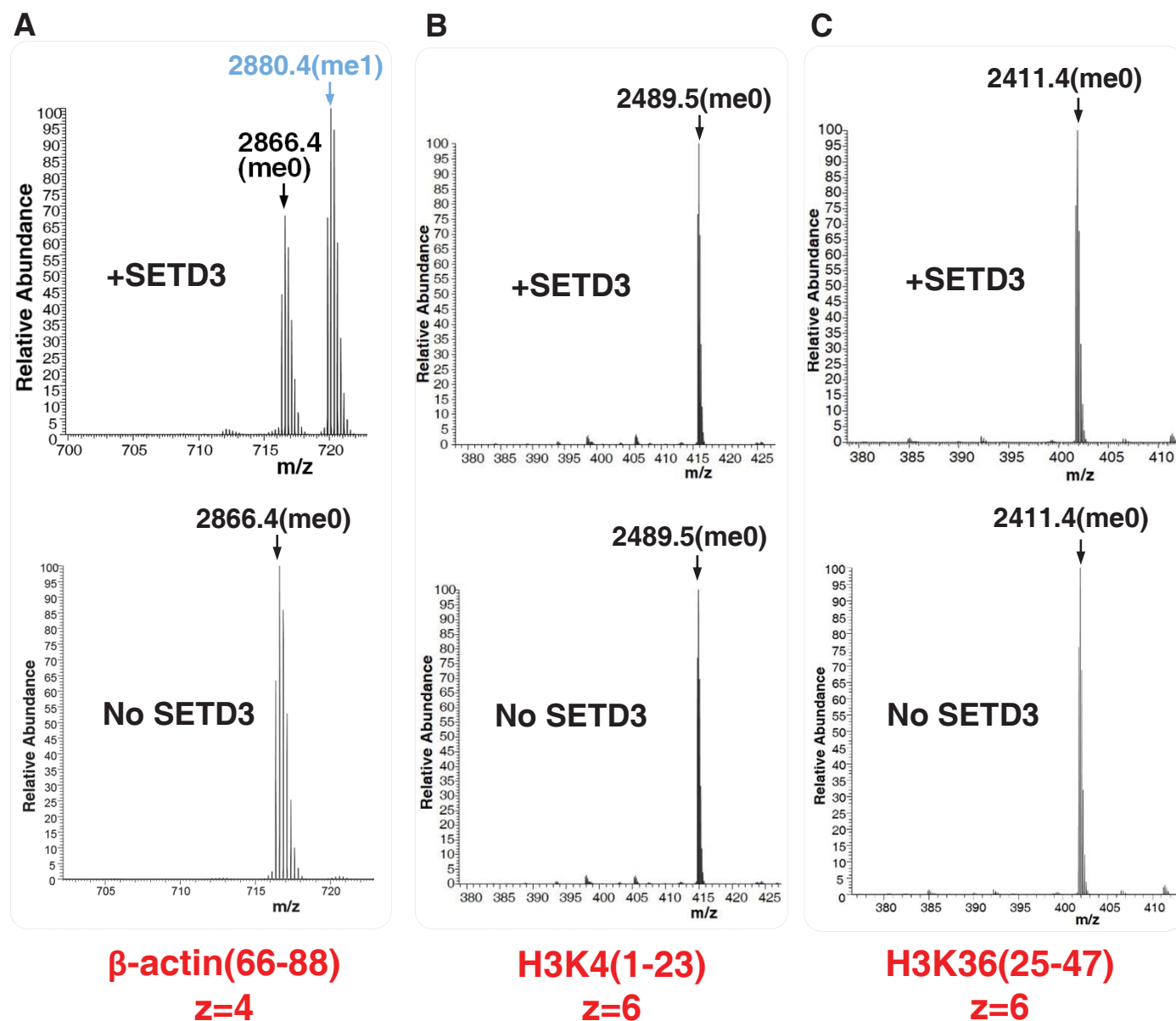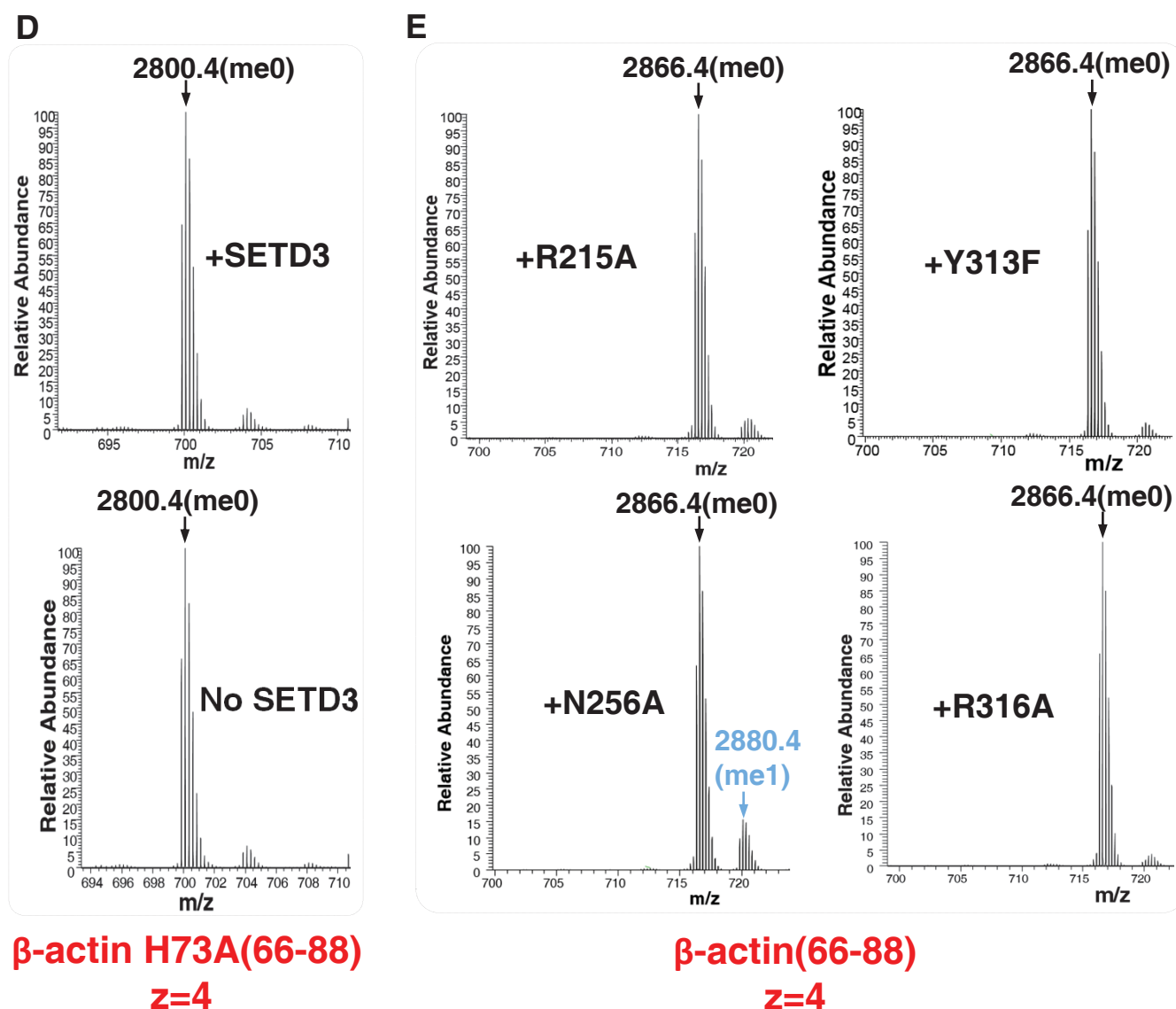CARNMT1-Carnosine (5YF1)
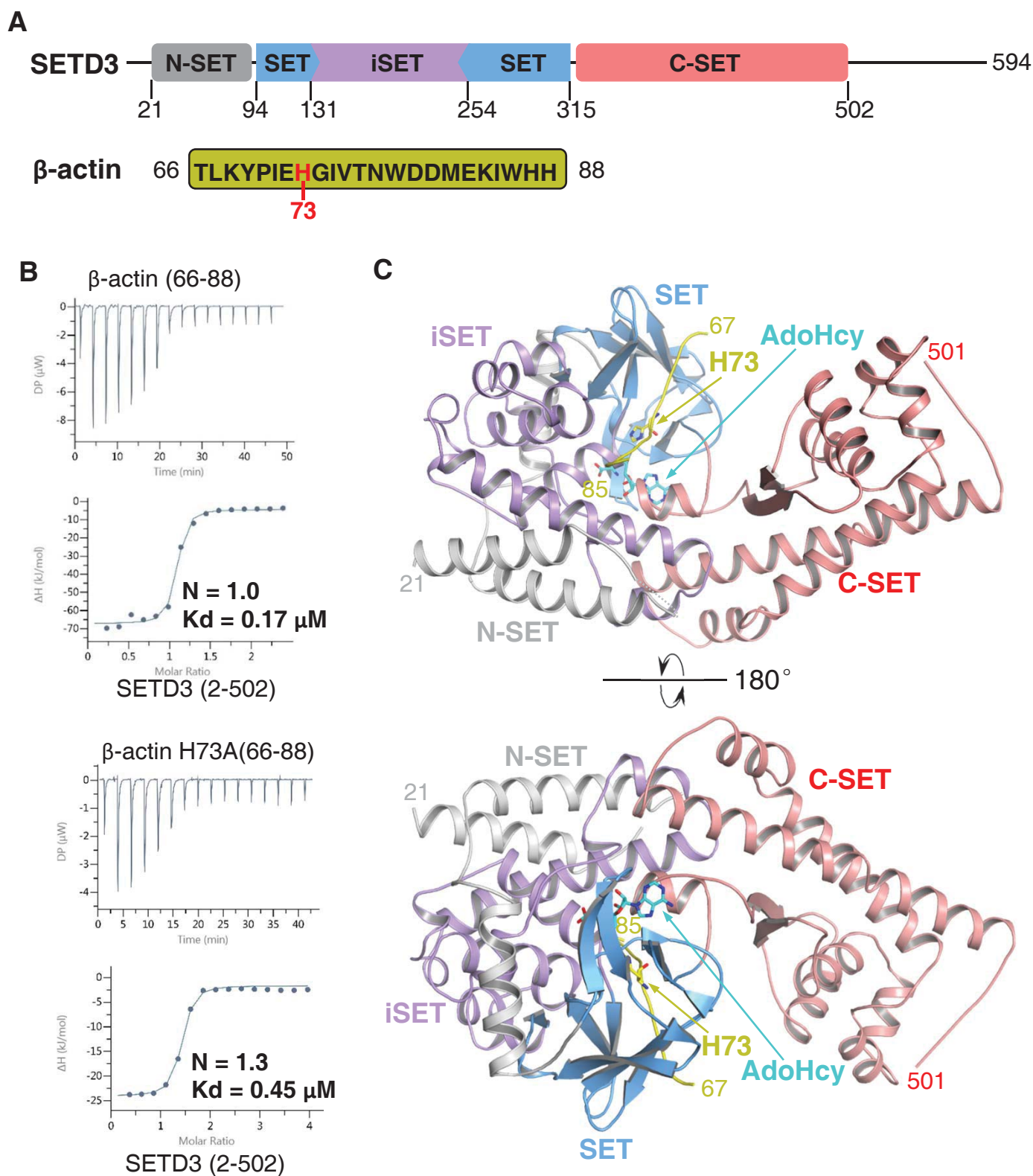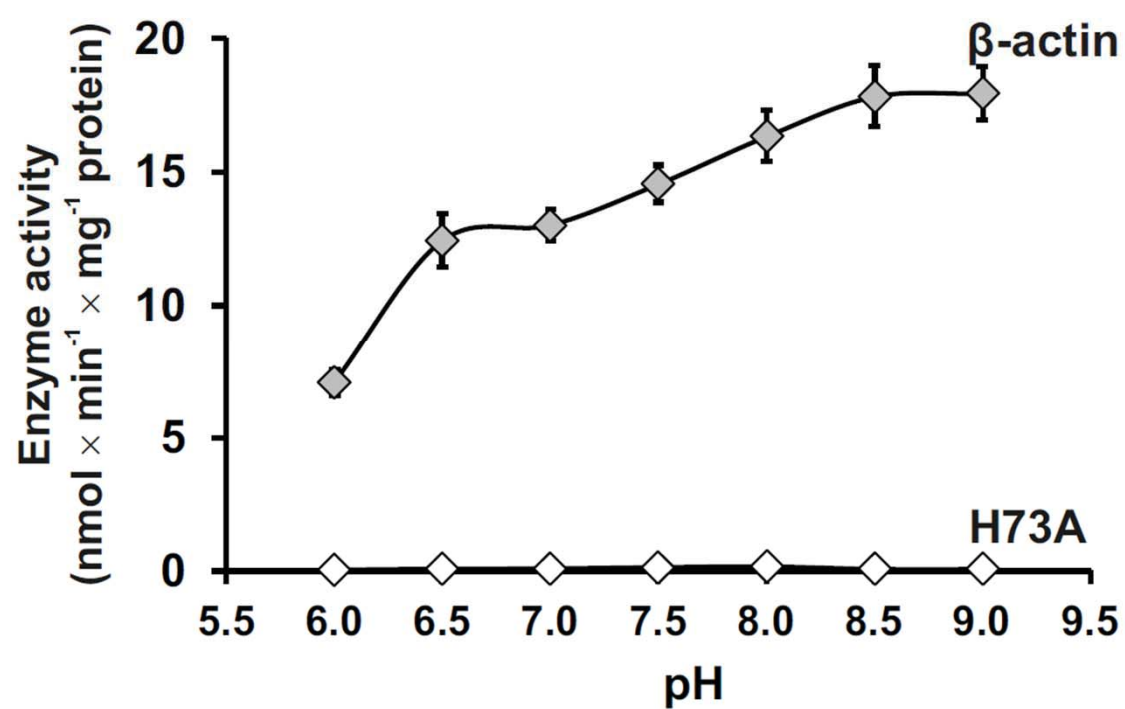
Figure 2

Figure 1–figure supplement 1 (To be continued)

Mass Spectrometry data showing the activity of SETD3 towards different peptides. Core region of SETD3 (2-502) methylates (A) the β-actin peptide (aa 66-88), but not (B) H3K4 (1-23), (C) H3K36 (25-47), or (D) β-actin H73A(66-88) (E) The activity of SETD3 mutants on the β-actin peptide (66-88).

Figure 1–figure supplement 1

A
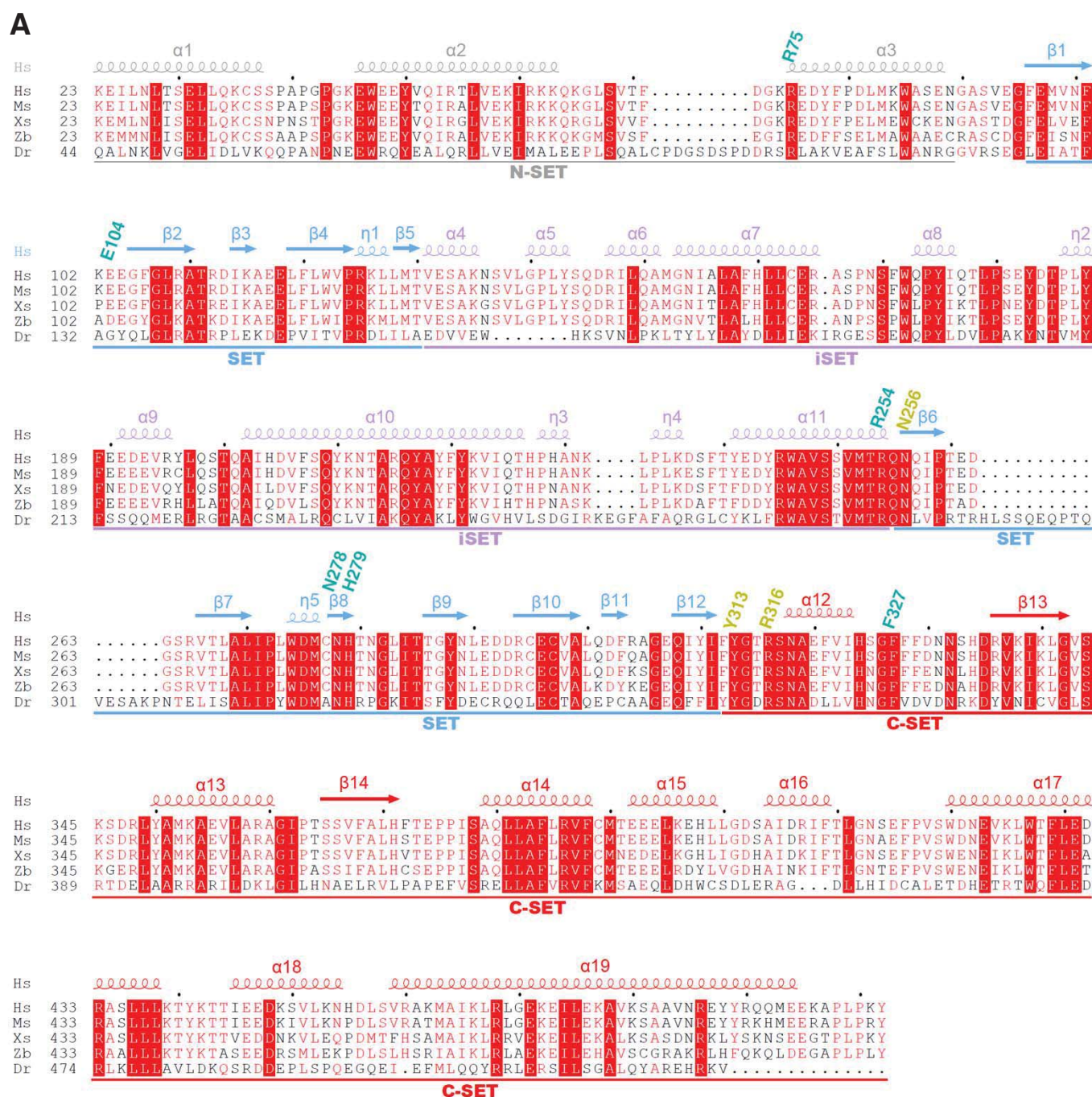
Figure 1–figure supplement 2 (To be continued)

B
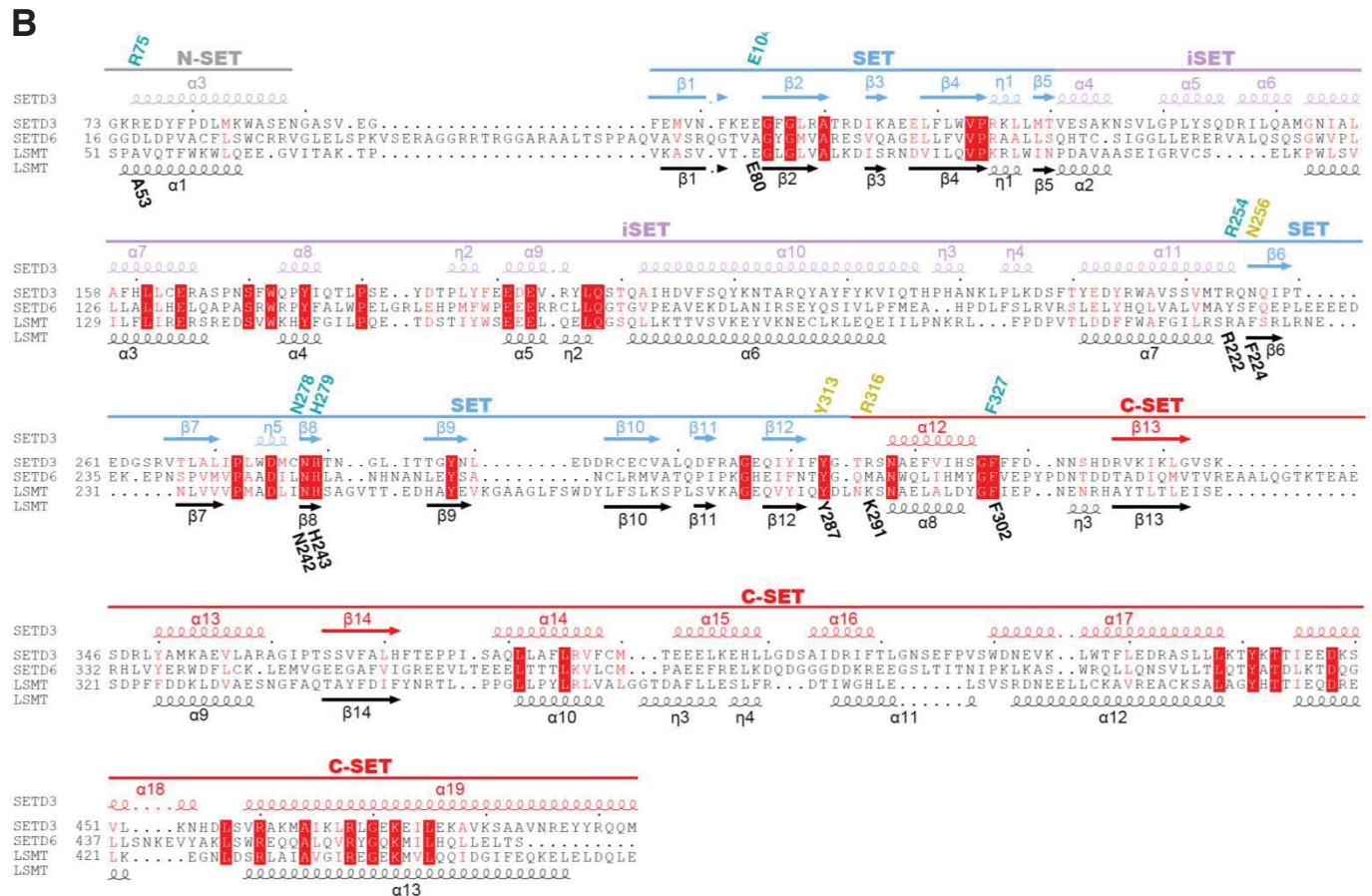
Sequence alignment of human SETD3 with its orthologs or other SET domain proteins (SETD6 and LSMT). (A) Sequence alignment of Human SETD3(Hs, NP_115609.2), mouse SETD3(Ms, NP_082538.2), Xenopus SETD3(Xs, NP_001016577), Zebrafish SETD3 (Zb, NP_956348.1) and Drosophila (Dr, XP_017048262.1). The secondary structures of human SETD3 are colored in the same way as shown in Figure 1A. The residues involved in binding to AdoHcy and His73 are labeled in cyan and yellow, respectively. (B) Sequence aligment of human SETD3, human SETD6 (NP_001153777.1) and *Pisum sativum* LSMT (AAA69903.1). The secondary structures, AdoHcy binding residues, and His73 binding residues, are labeled in the same way as shown in Figure 1–figure supplement 2A.

Figure 1–figure supplement 2
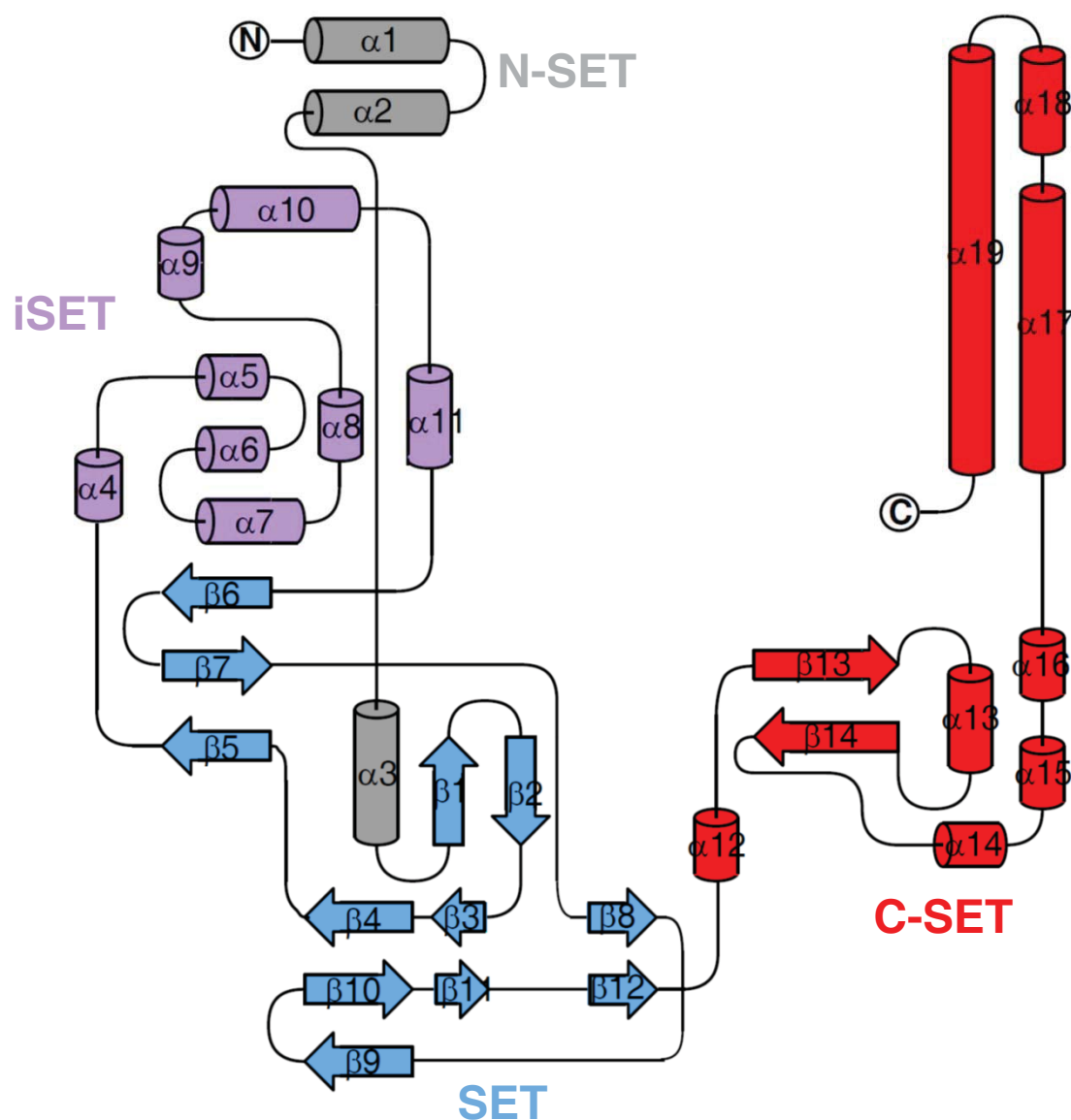
Topology of SETD3 (2-502), with secondary structures marked and colored in the same way as shown in Figure 1–figure supplement 2A.

Figure 1–figure supplement 3

A

C

H73me

N

AdoHcy

SETD3-AdoHcy-methylated β-actin
SETD3-AdoHcy-methylated β-actin
SETD3-AdoHcy-methylated β-actin
SETD3-AdoHcy-methylated β-actin

B

C

H73

N

AdoHcy

SETD3-AdoHcy-β-actin
SETD3-AdoHcy-β-actin
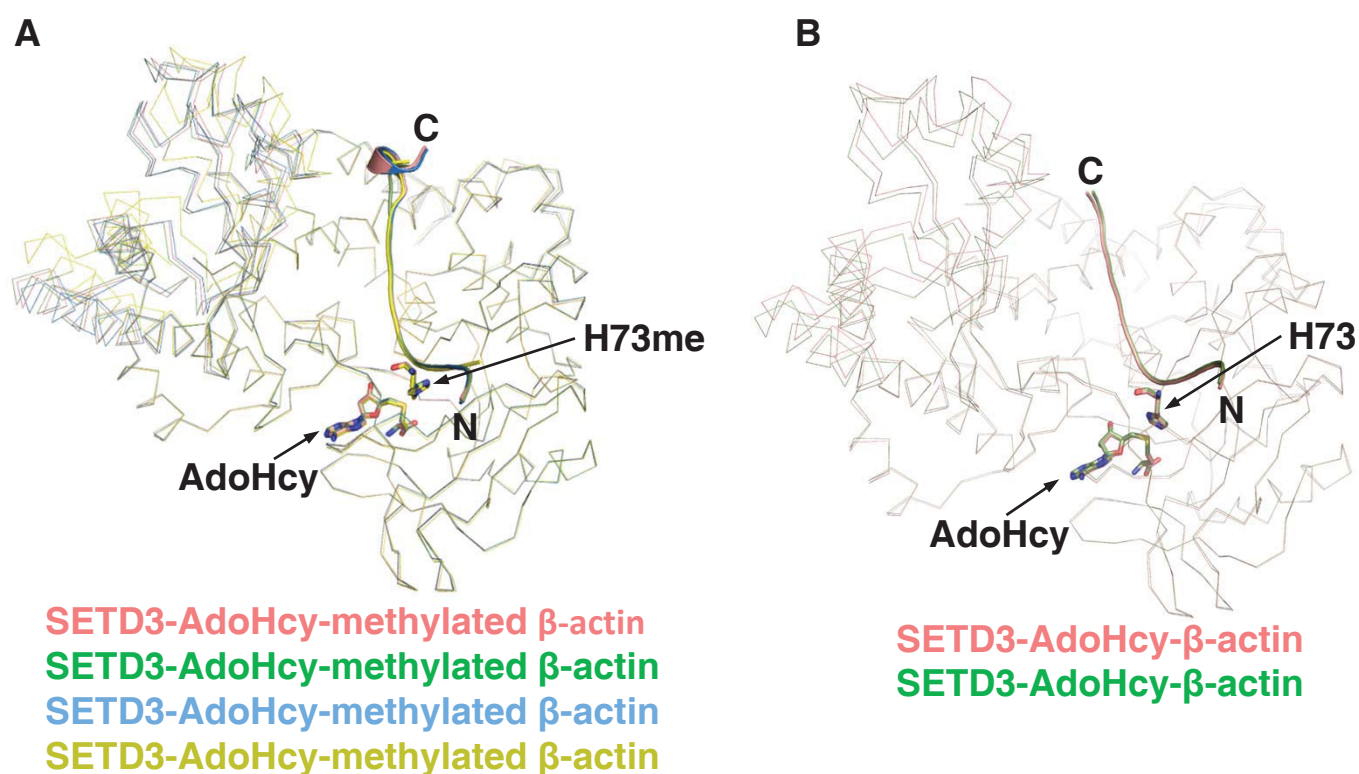
Superposition of SETD3 molecules. (A) Superposition of four SETD3 molecules bound to methylated β-actin in the same asymmetric unit, with the four molecules shown in red, green, blue and yellow ribbon, respectively. His73me of β-actin and AdoHcy are shown in sticks. (B) Superposition of two molecules of SETD3 bound to unmodified β-actin in the same asymmetric unit, with the two molecules shown in red and green ribbon, respectively. His73 of β-actin and AdoHcy are shown in sticks.

Figure 1–figure supplement 4
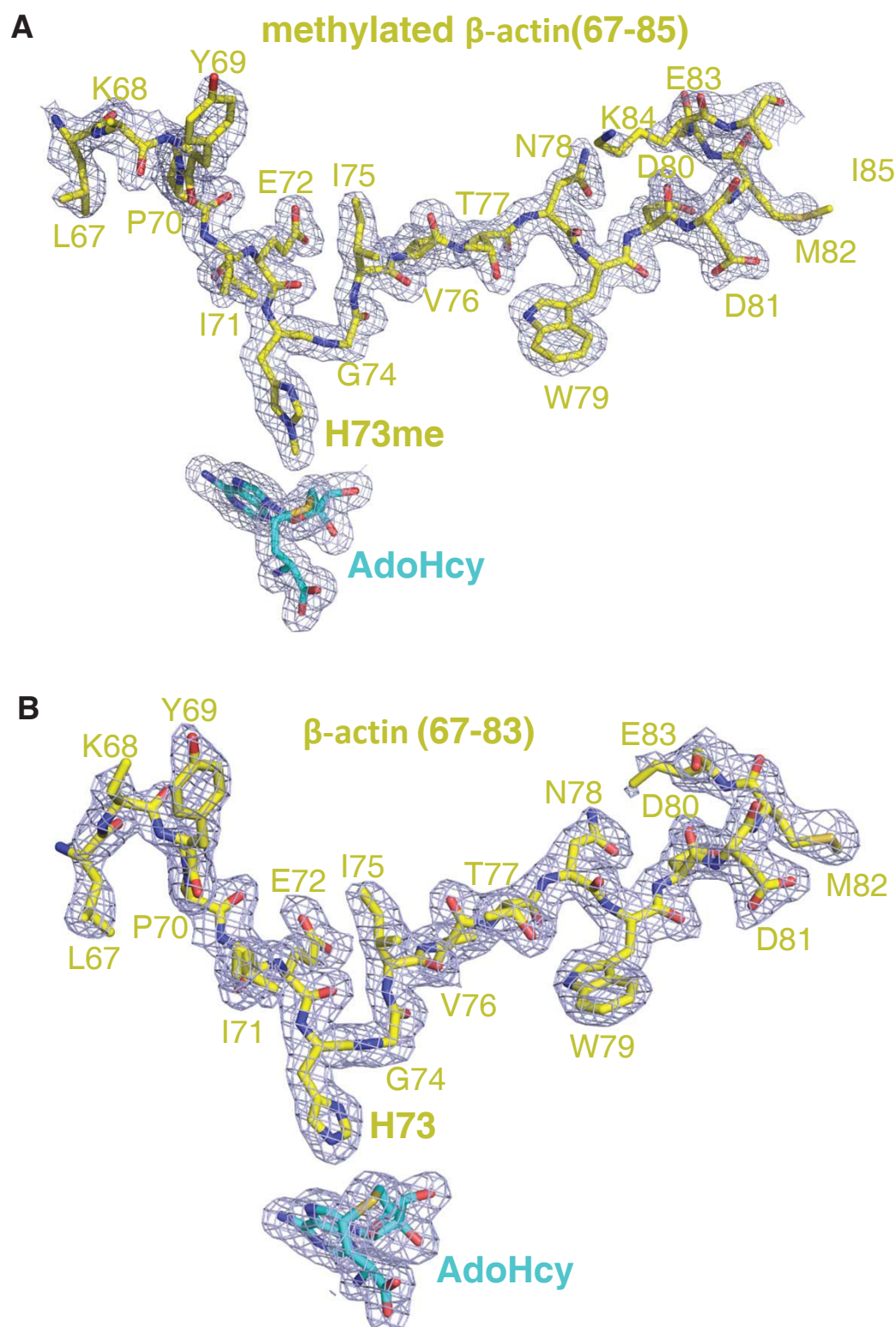
The 2|Fo|–|Fc| σ-weighted maps of (A) methylated β-actin peptide and (B) unmodified β-actin peptide in the presence of AdoHcy, are contoured at 1.2 σ (blue cage), respectively. The peptides are shown in yellow sticks.
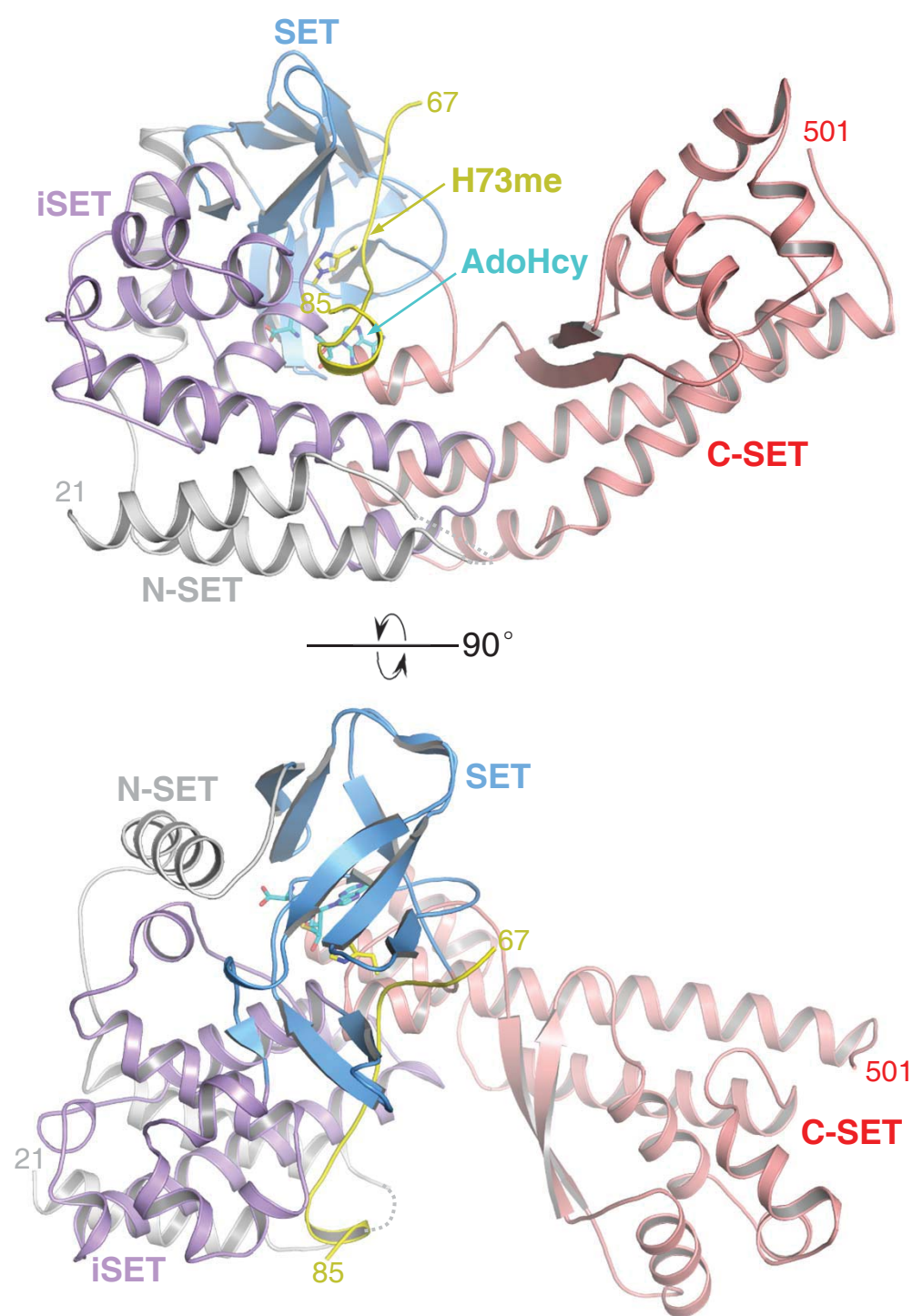
Figure 1–figure supplement 5
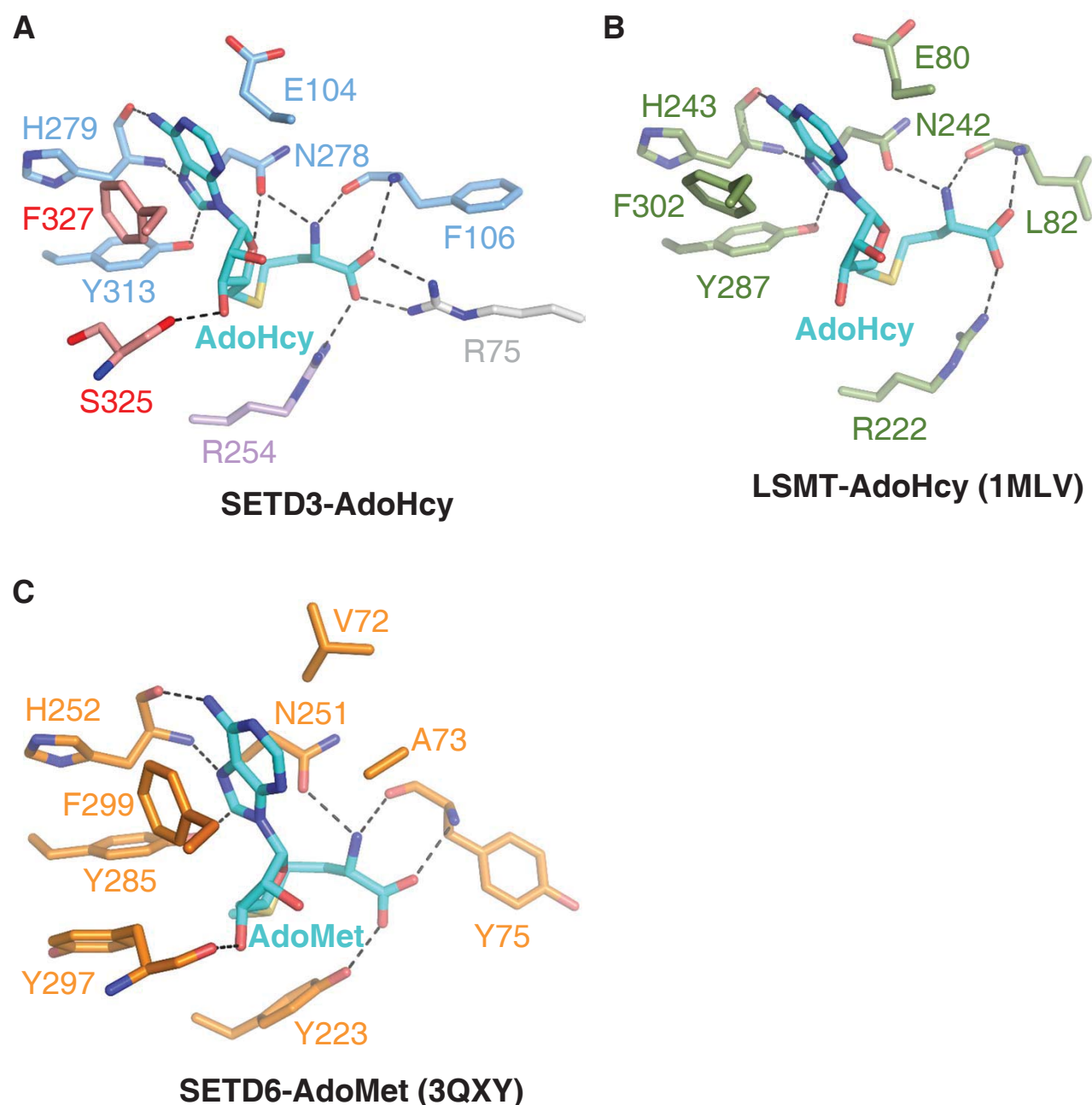
Comparison of AdoHcy binding mode of SETD3 with those observed in LSMT and SETD6. (A) A detailed depiction of intermolecular interactions between SETD3 and AdoHcy, with AdoHcy shown in cyan sticks, and the AdoHcy binding residues of SETD3 shown in sticks and colored in the same mode as in Figure 1A. (B) Detailed interactions between AdoHcy and LSMT (PDB id: 1MLV), with AdoHcy binding residues of LSMT and AdoHcy shown in green and cyan sticks, respectively. (C) Detailed interactions between AdoMet and SETD6 (PDB id: 3QXY), with AdoMet binding residues of SETD6 and AdoMet shown in orange and cyan sticks, respectively. In Figures 2B and 2C, hydrogen bonds are indicated by black dashes.

Figure 1–figure supplement 6
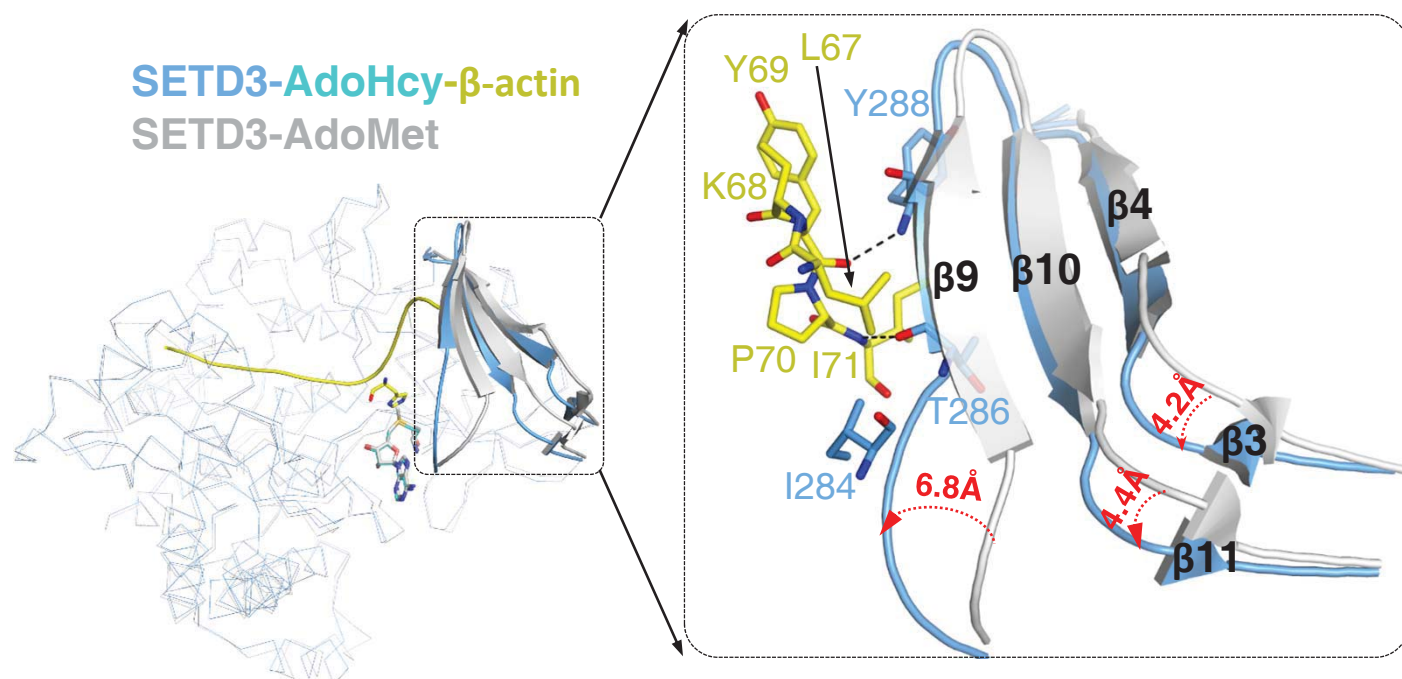
Superposition of AdoMet-bound SETD3 (PDB id: 3SMT) with AdoHcy bound SETD3-actin. In the structure of AdoMet bound SETD3, the protein is shown in grey ribbon and AdoMet is shown in grey sticks. In the structure of AdeHcy bound SETD3 in the presence of actin, protein is shown in blue ribbon and AdoHcy is shown in yellow sticks. β4-β9-β10 and β3-β11 changed conformations significantly upon binding to actin peptide, which are shown in cartoon representation. Leu67-Ile71 of β-actin and their interaction residues in SETD3, are shown in sticks. Three loops that precede β4, β9 and β11 shift 4.2Å, 4.4Å, and 6.8Å, respectively.

Figure 1–figure supplement 7

Overall structure of SETD3 with methylated β-actin peptide in the presence of AdoHcy. SETD3 is colored and labelled in the same mode as shown in Figure 1C. AdoHcy and His73me are shown in sticks.

**Figure 1–figure supplement 8**
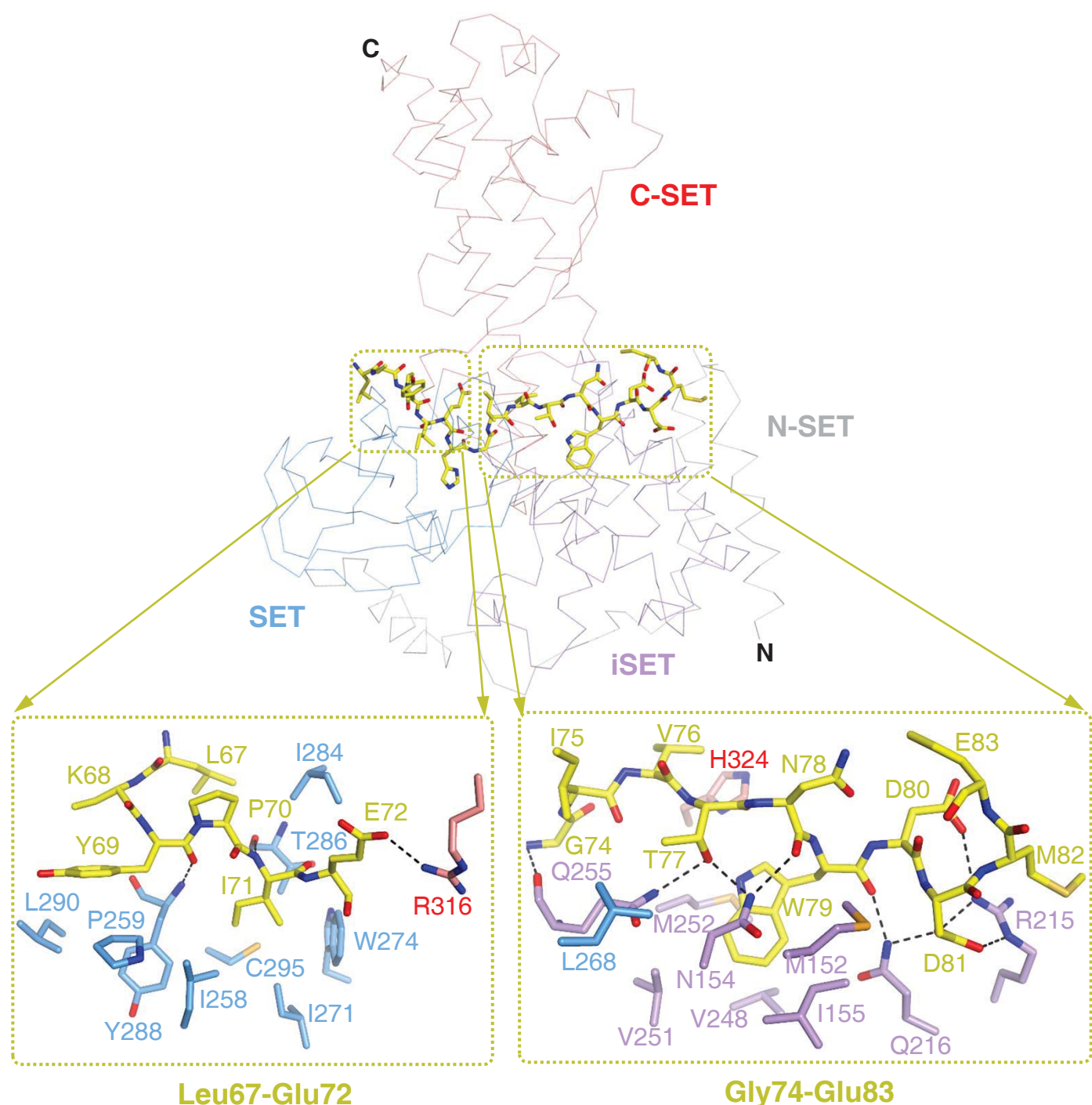
Detailed interactions of SETD3 and β-actin peptide (66-88). The β-actin peptide mainly contacts N-terminal lobe of SETD3, with its N-terminal and C-terminal sides contact SET and iSET domains, respectively. In the top panel, SETD3 are shown in ribbon and colored in the same way as shown in Figure 2A. β-actin peptide is shown in yellow sticks. Detailed interactions between SETD3 and Leu67-Glu72, and between SETD3 and Gly74 and Glu83, are shown in the left bottom and right bottom panels, respectively. The SETD3 residues involved in β-actin binding are shown in sticks.

Figure 2–figure supplement 1
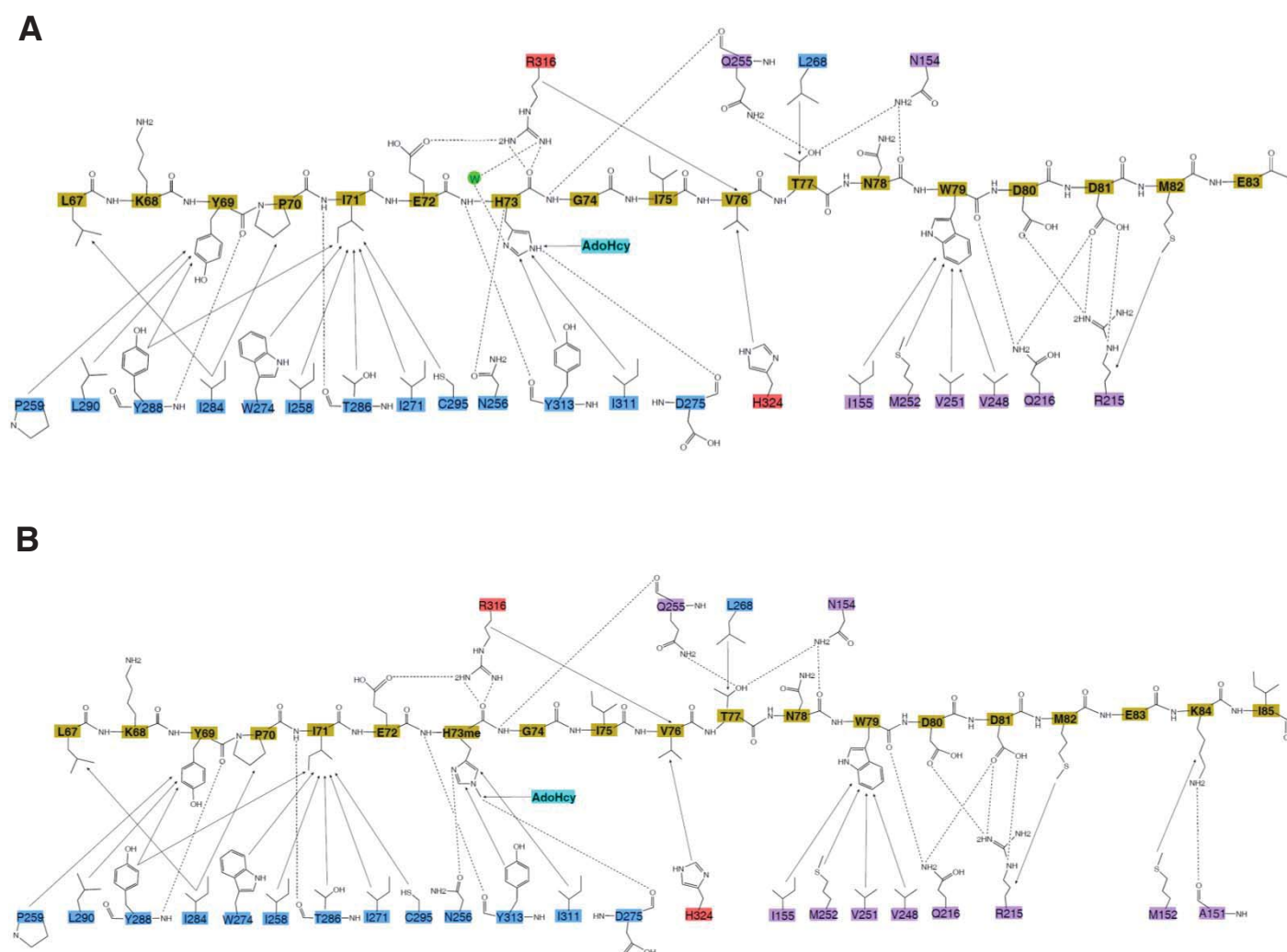
Schematic of the detailed interactions (A) between SETD3 and unmodified β-actin (B) and between SETD3 and methylated β-actin. SETD3 residues are colored as shown in Figure 1A, while the peptide residues are colored in yellow. The hydrophobic interactions and hydrogen bonds between protein and peptide are shown in black solid arrows and black dash arrows, respectively.

Figure 2–figure supplement 2
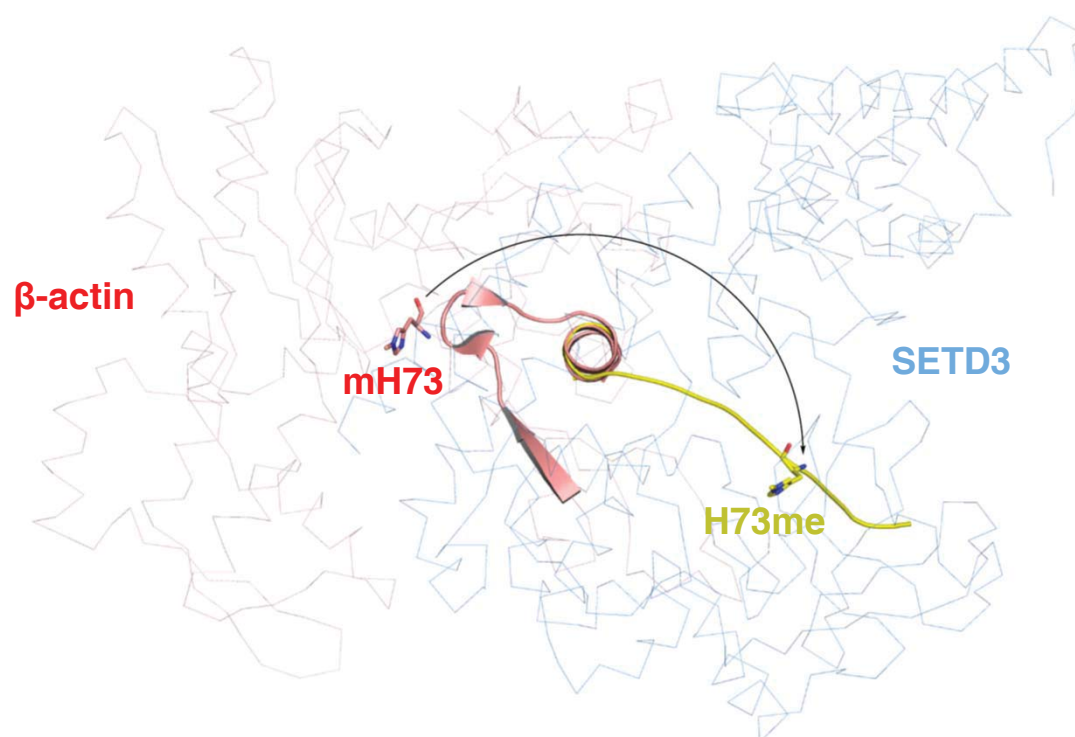
Actin endures conformational changes upon binding to SETD3. β-actin peptide (66-88, yellow cartoon) is over laid with the same fragment in the structure of native β-actin (red cartoon) (PDB id: 1HLU). native β-actin decomposes its local secondary structures upon SETD3 binding. Native β-actin and SETD3 are shown in red and blue ribbon, respectively.

Figure 2–figure supplement 3